PHILOSOPHICAL TRANSACTIONS OF THE ROYAL SOCIETY A MATHEMATICAL, PHYSICAL & ENGINEERING SCIENCES

Volcanic Rocks of the 1985 Tibet Geotraverse: Lhasa to Golmud

Julian A. Pearce and Mei Houjun

Phil. Trans. R. Soc. Lond. A 1988 **327**, 169-201
doi: 10.1098/rsta.1988.0125

Phil. Trans. R. Soc. Lond. A **327**, 169–201 (1988) [169]
Printed in Great Britain

Volcanic rocks of the 1985 Tibet Geotraverse: Lhasa to Golmud

By Julian A. Pearce[1] and Mei Houjun[2]

[1] *Department of Geology, The University, Newcastle-upon-Tyne, U.K.*
[2] *Institute of Geochemistry, Chinese Academy of Sciences, Guiyang, People's Republic of China*

[Microfiche in pocket]

Volcanic rocks encountered during the Tibet Geotraverse have been studied in the field, in thin section and by major and trace element geochemistry in order to determine their most probable original eruptive environment. Rocks from a total of eleven distinct volcanic provinces were studied in this way. They provide evidence for: an active continental margin or post-collision province of probable Devonian/early Carboniferous age in the northern Kunlun mountains; an active continental margin of late Carboniferous age in the southern Lhasa Terrane; Permian continental rifts in the central Qiangtang and central Kunlun Terranes; Triassic volcanic arcs in the southern Lhasa and northern Qiangtang Terranes; a Triassic active continental margin dyke swarm in the northern Kunlun mountains; a Jurassic post-collision or back-arc rifting province in the southern Qiangtang Terrane; a Jurassic island arc in the northern Lhasa Terrane; a Cretaceous post-collision province in the northern Lhasa Terrane possibly extending into the southern Qiangtang Terrane; and a Palaeogene active continental margin in the southern Lhasa Terrane. An Oligocene trachyte plug in the northern Qiangtang Terrane was the only evidence encountered during the Geotraverse of volcanism post-dating the Palaeogene India–Eurasia collision. However, the composition of this plug, coupled with new and published analyses from Miocene volcanics in the southern Lhasa terrane and from the Pliocene-Recent volcanic province of northwest Tibet, places important constraints on models for post-collision underplating of Tibet by continental lithosphere: any underplating is likely to have been (*a*) much later than the start of collision, (*b*) directed beneath Tibet from the north as well as the south, and (*c*) limited in extent.

1. Introduction

Volcanic rocks can contribute to our understanding of the Tibetan Plateau in two ways: they can provide information on past tectonic environments as an aid to the palaeo-tectonic reconstruction of the plateau and, in the case of the more recent eruptions, they can place constraints on tectonic models for the India–Eurasia continent-continent collision event. Use of a sequence of volcanic rocks to interpret a past tectonic environment can best be achieved by the systems approach, whereby geochemical fingerprinting techniques are integrated with information on primary and secondary mineralogy, the facies of the intercalated sediment, the types of eruption, the proportions of rock types erupted and a variety of geological criteria such as the nature of associated rock types and of the basement to the volcanic sequence. Use of volcanic rocks to understand continent collision is based on the time–space relationships of syn- and post-collision magmatism, on geochemical and petrologic evidence for the nature of the magma source region and on the type and degree of subsequent crustal interaction. Because few post-(Palaeogene) collision volcanics were collected on this Geotraverse, the principal aim

of this paper is to provide new information on the past tectonic environments of the Geotraverse region; however, an attempt has also been made to compile new and published data relevant to the neotectonics of the Tibetan Plateau.

Eleven volcanic provinces were identified during the Geotraverse (figure 1). For each province, the geological setting and volcanic stratigraphy were studied in as much detail as time permitted for one or more volcanic sequences and a representative suite of samples was collected. In general, 'G' numbers were collected and analysed by the Royal Society group and sample locations are given in Kidd *et al.*, this volume (field slip, microfiche 2, in pocket); 'Qy' numbers were collected and analysed by the Chinese group, and sample locations are

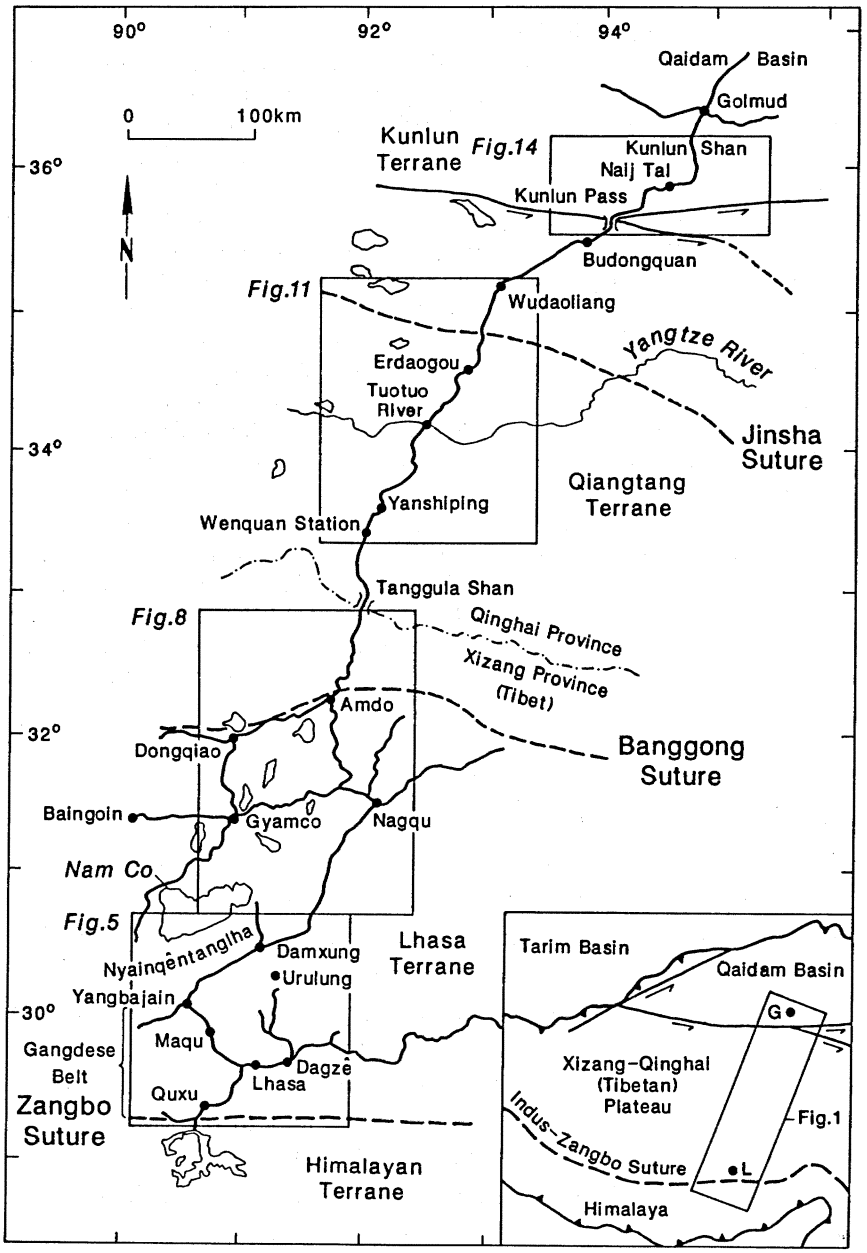

FIGURE 1. Route taken by Geotraverse also showing the location of the larger scale maps in figures 5, 8, 11 and 14.

available from Mei Houjun on request. Subsequently, about 150 samples were examined in thin section and analysed for major elements and a range of trace elements. In this paper, we start by explaining the methodology used; we then report the geological, petrological and geochemical characteristics of each of the provinces studied and discuss the tectonic implications of the data; finally we summarize our results in the context of the evolution of the Tibetan Plateau. This paper concentrates on the non-ophiolitic volcanic rocks and related hypabyssal intrusions, whereas Pearce & Deng (this volume) examine in more detail the ophiolite environments.

2. Methodology

Our main basis for the interpretation of past eruptive environments is geochemical. All samples have been analysed by atomic absorption spectroscopy (AAS) for the major elements, either in Newcastle or in Guiyang. Samples analysed at Newcastle were also analysed for the trace elements Zr, Y, Nb, Rb, Sr and Th by X-ray fluorescence (XRF) and for Cr, Ni, V, Cu, Zn, and Sc by AAS. A representative subset of about 40 samples was also analysed for the rare earth elements (REE), Th, Ta, Hf, Sc and Co by instrumental neutron activation analysis (INAA) at the Open University, at the Institut Laue-Langevin, Grenoble and at the Third Institute of the Department of Nuclear Industry in Beijing. Some additional data on REE and some other elements were obtained by inductively-coupled plasma emission spectrometry (ICP–AES) at the Central Laboratory of Geology in Hebei. Analyses of comparable rocks were analysed in several laboratories to confirm inter-laboratory compatibility. A table of representative data is presented as table 1 and the full data set is published in the Appendix (microfiche 1, in pocket).

Since most of the rocks studied during the traverse were affected by alteration/metamorphism, tectonic classification has in general been restricted to those elements that have been demonstrably immobile since eruption. Classification of rock type has, however, been carried out for orogenic series using the K_2O–SiO_2 diagram of Peccerillo & Taylor (1976), although care was taken not to plot analyses when covariation diagrams of K_2O against immobile elements indicated that potassium had been significantly mobile. The classification of rock type for non-orogenic series was carried out using the Ti/Zr–Nb/Y diagram of Winchester & Floyd (1977), since all available samples of this type were too altered for conventional diagrams such as total alkalis–silica to be used reliably. Classification of tectonic setting has been carried out using MORB-normalized multi-element patterns (Pearce 1984) coupled with the two discrimination diagrams, Ti–Zr–Y (Pearce & Cann 1973) and Th–Ta–Hf (Wood *et al.* 1979). Additional diagrams, such as REE patterns, have been used to examine petrogenetic relationships between rocks, where this is relevant to the tectonic interpretation.

The rationale behind the geochemical techniques is illustrated in figures 2 and 3. The MORB-normalized patterns shown in figure 2 are based on single analyses of basalts, in which the elements Th–Yb are arranged from right to left in order of increasing incompatibility during mantle melting; these patterns resemble those shown in Pearce (1984) except that the mobile elements have been removed from consideration. Figures 2*a–d* show some typical patterns from the various eruptive environments for comparison with the patterns to be presented for the Tibetan samples. Figure 2*a* shows the range of patterns characteristic of oceanic and continental intraplate basalts: they exhibit an enrichment relative to normal MORB for all elements except Y and Yb, a feature that can be explained by derivation from enriched mantle sources (e.g.

TABLE 1. GEOCHEMICAL ANALYSES FOR REPRESENTATIVE SAMPLES OF VOLCANIC ROCKS FROM THE GEOTRAVERSE

(Elements Zr, Y, Nb, Sr and Rb have been analysed by X-ray fluorescence, elements Hf to Lu by instrumental neutron activation analysis, and the remaining elements by atomic absorption. Zr and Nb in Qy numbers are estimated from Hf (Zr = Hf × 37.5) and Ta (Nb = Ta × 16) respectively. Unanalysed elements are given as 0. Key to rock sequences: L = Lhasa Terrane; Q = Qiangtang Terrane; K = Kunlun terrane; T = Tibet; Cb = Carboniferous ; P = Permian; T = Triassic; J = Jurassic; C = Cretaceous; Pg = Palaeogene; Q = Quaternary; U = Upper; L = Lower. Key to rock types: bas. = basalt; and. = andesite; b/a. = basaltic andesite; sho. = shoshonite; p/b. = picrite basalt; rhy. = rhyolite; tra. = trachyte; bsn. = basanite; phn. = phonolite; L = lava; D = dyke; P = plug; S = sill; PL = pillow lava. See figures 5, 8, 11 and 14 for province locations and Kidd *et al.*, this volume (field slips, Microfiche 2, in pocket) and Deng 1978 for precise locations and phenocryst mineralogies).

Samp.	G16E	G32G	G36C	G46C	G106D	G130E	G55G	G99B	OPH474
Seq.	LCb1	LT1	LPg1	LPg2	LJ1	LJ2	LC1	LC2	LC3
Rock	bas.	bas.	b/a.	sho.	bas.	bas.	b/a.	b/a.	bas.
Type	L	L	L	L	PL	L	L	L	L
SiO_2	52.00	48.70	53.20	53.50	47.60	49.50	53.50	53.60	51.83
TiO_2	1.03	0.92	0.83	0.84	0.56	0.52	0.87	0.94	1.56
Al_2O_3	17.00	14.60	21.00	19.70	11.20	14.30	15.20	15.80	16.21
Fe_2O_3	9.06	7.94	6.52	6.22	6.20	8.83	8.35	8.09	8.77
MnO	0.17	0.17	0.07	0.13	0.15	0.15	0.13	0.13	0.21
MgO	5.74	4.39	3.33	1.75	5.04	7.44	7.85	3.93	4.68
CaO	9.61	10.80	7.34	4.27	15.90	12.60	8.92	7.01	5.38
Na_2O	3.95	2.14	4.99	4.12	3.51	1.23	2.35	2.79	4.05
K_2O	0.10	1.05	0.42	6.00	0.68	0.18	1.67	2.13	2.80
P_2O_5	0.23	0.25	0.16	0.42	0.09	0.07	0.19	0.17	0.04
LOI	1.41	9.31	2.69	3.60	9.98	3.77	1.68	5.65	3.75
Total	100.30	100.27	100.55	100.55	100.91	98.59	100.71	100.24	99.28
Zr	88	125	146	401	32	33	109	158	142
Y	22	23	17	35	11	13	20	26	28
Nb	5.8	3.9	5.0	24.0	2.4	2.2	6.6	10.0	10.0
Rb	2.8	49.0	8.5	142.0	13.0	0.0	71.0	91.0	66.0
Sr	502	914	603	99	157	324	309	434	830
Cr	150	83	35	2	480	220	460	57	110
Ni	39	16	21	8	217	58	83	16	37
V	290	210	190	88	180	0	220	0	355
Cu	21	15	30	42	35	118	17	32	42
Zn	83	82	100	93	51	68	76	94	0
Hf	2.09	3.33	3.16	7.57	0.91	1.01	2.49	4.00	3.78
Ta	0.37	0.24	0.41	1.82	0.11	0.14	0.53	0.93	0.65
Th	2.00	17.00	5.52	42.40	0.69	0.54	11.40	15.60	13.20
Sc	35.0	0.0	21.0	7.1	27.1	40.8	29.0	22.1	0.0
Co	32.7	28.0	25.8	34.0	34.8	44.0	37.1	32.5	0.0
La	12.2	0.0	15.2	83.1	3.6	3.7	23.7	30.2	41.5
Ce	26.9	0.0	28.4	171.0	9.5	11.0	46.2	66.1	66.3
Nd	16.9	0.0	15.6	69.0	5.8	10.3	23.2	33.0	28.3
Sm	4.05	0.00	3.52	12.50	1.50	2.17	4.97	5.95	5.57
Eu	1.25	0.00	1.10	2.93	0.52	0.75	1.25	1.35	1.47
Tb	0.67	0.00	0.59	1.67	0.36	0.40	0.73	0.89	0.80
Ho	0.00	0.00	0.00	2.07	1.00	0.59	0.00	1.18	0.00
Tm	0.00	0.00	0.00	0.59	0.16	0.19	0.00	0.44	0.00
Yb	2.22	0.00	1.70	3.39	1.33	1.56	1.93	2.70	1.87
Lu	0.38	0.00	0.28	0.46	0.23	0.27	0.32	0.41	0.29

PHILOSOPHICAL TRANSACTIONS OF THE ROYAL SOCIETY A MATHEMATICAL, PHYSICAL & ENGINEERING SCIENCES

TABLE 1. (*cont.*)

Samp.	OPH585	G133H	G138H	G151D	Qy61	Qy59	Qy71	Qy78B	Qy77B
Seq.	LC3	LC4	QJ1	QP1	QP1	QP1	QP1	QP2	QP2
Rock	and.	b/a.	b/a.	bas.	bas.	and.	p/b.	b/a.	and.
Type	L	L	L	L	S	L	L	L	L
SiO_2	61.15	54.40	53.10	50.10	47.53	62.86	45.91	53.39	59.38
TiO_2	0.84	2.12	1.64	1.60	2.24	0.54	1.12	0.94	0.66
Al_2O_3	15.73	15.70	16.80	17.30	14.48	16.76	17.68	18.29	18.28
Fe_2O_3	7.01	8.76	11.10	9.53	12.77	5.19	8.99	6.70	4.95
MnO	0.10	0.18	0.06	0.16	0.46	0.20	0.16	0.18	0.12
MgO	3.86	3.39	5.36	5.42	5.10	5.00	7.17	4.80	1.70
CaO	1.09	8.25	2.00	7.78	11.20	3.70	9.82	5.00	2.30
Na_2O	4.63	3.71	5.83	4.83	1.85	4.54	4.03	5.44	8.70
K_2O	2.25	1.03	0.48	0.38	0.68	0.19	0.03	1.30	0.75
P_2O_5	0.08	0.35	0.49	0.43	0.22	0.12	0.30	0.52	0.38
LOI	2.98	3.04	3.93	3.22	2.94	1.00	2.00	3.55	1.82
Total	99.72	100.93	100.79	100.75	99.47	100.10	97.98	100.11	99.04
Zr	180	307	187	149	136	109	112	191	129
Y	23	36	25	25	44	11	26	24	17
Nb	16.0	11.0	11.0	15.0	15.0	11.0	14.0	35.0	8.0
Rb	130.0	29.0	21.0	8.6	7.0	4.0	1.0	33.0	0.0
Sr	450	334	131	613	475	498	160	1133	0
Cr	0	45	200	124	0	0	0	0	0
Ni	80	12	59	94	0	0	0	0	0
V	0	210	280	230	0	0	0	0	0
Cu	41	17	8	9	0	0	0	0	0
Zn	0	140	83	90	0	0	0	0	0
Hf	4.80	6.14	3.63	3.21	3.62	2.91	3.00	5.10	3.46
Ta	0.99	0.88	0.70	0.89	0.95	0.74	0.83	2.17	0.49
Th	19.60	8.40	3.89	2.12	1.00	4.10	1.90	7.30	6.00
Sc	0.0	26.3	18.8	26.5	58.2	23.9	30.0	22.4	13.6
Co	0.1	29.1	30.5	37.5	0.0	0.0	0.0	0.0	0.0
La	30.4	23.7	14.0	22.2	10.5	14.0	19.5	45.3	42.0
Ce	66.9	58.2	37.7	52.4	27.3	25.5	36.0	95.3	69.2
Nd	25.2	32.6	21.5	27.3	19.5	12.9	18.2	39.9	27.0
Sm	5.59	7.08	4.72	5.19	6.60	2.80	5.10	8.10	5.00
Eu	1.25	2.15	1.47	1.79	2.05	0.79	1.26	1.54	1.37
Tb	0.70	1.20	0.80	0.83	1.10	0.45	0.91	0.82	0.60
Ho	0.00	1.85	0.00	1.30	0.00	0.00	0.00	0.00	0.00
Tm	0.00	0.48	0.37	0.32	0.00	0.00	0.00	0.00	0.00
Yb	2.18	4.09	2.42	2.53	4.80	1.00	2.40	1.10	1.00
Lu	0.38	0.57	0.35	0.41	0.62	0.15	0.27	0.30	0.17

Samp.	G154F	G154L	Qy80	Qy85	G216I	Qy171	Qy154	Qy181	Qy206
Seq.	QT1U	QT1L	QT2	QT2	KP1	KD1	KD1	KD1	KD1
Rock	bas.	bas.	bas.	and.	bas.	dac.	latite	rhy.	rhy.
Type	L	L	L	L	L	L	L	L	L
SiO_2	51.30	51.50	51.75	56.91	47.20	63.28	68.48	70.28	77.11
TiO_2	1.00	0.78	0.76	0.66	3.54	0.66	0.36	0.40	0.14
Al_2O_3	18.80	21.40	19.35	18.44	14.40	17.38	15.61	16.01	11.43
Fe_2O_3	9.07	7.99	8.67	10.79	14.90	5.33	4.81	2.55	1.87
MnO	0.23	0.12	0.19	0.08	0.19	0.07	0.08	0.07	0.09
MgO	3.58	2.60	2.87	0.40	5.46	3.30	0.60	0.20	0.10
CaO	8.72	9.94	6.55	1.80	10.10	2.60	1.80	1.00	0.30
Na_2O	3.14	3.62	5.20	9.50	2.58	2.70	1.31	7.70	2.76

PHILOSOPHICAL TRANSACTIONS OF THE ROYAL SOCIETY A MATHEMATICAL, PHYSICAL & ENGINEERING SCIENCES

TABLE 1. (*cont.*)

Samp.	G154F	G154L	Qy80	Qy85	G216I	Qy171	Qy154	Qy181	Qy206
Seq.	QT1U	QT1L	QT2	QT2	KP1	KD1	KD1	KD1	KD1
Rock	bas.	bas.	bas.	and.	bas.	dac.	latite	rhy.	rhy.
Type	L	L	L	L	L	L	L	L	L
K_2O	2.63	0.46	0.81	0.11	0.73	2.45	4.81	1.15	4.26
P_2O_5	0.45	0.09	0.14	0.10	0.34	0.22	0.24	0.14	0.08
LOI	2.20	1.81	2.73	1.09	0.78	1.67	0.97	0.63	1.93
Total	101.12	100.31	99.02	99.88	100.22	99.66	99.07	100.13	100.07
Zr	207	108	42	59	257	276	402	123	299
Y	25	26	18	13	36	46	37	16	74
Nb	25.0	4.1	4.0	5.0	23.0	16.0	21.0	19.0	20.0
Rb	101.0	6.1	18.0	3.0	18.0	132.0	283.0	43.0	178.0
Sr	526	141	279	174	152	131	39	72	18
Cr	6	7	0	0	240	0	0	0	0
Ni	12	7	0	0	125	0	0	0	0
V	240	280	0	0	430	0	0	0	0
Cu	38	17	0	0	198	0	0	0	0
Zn	103	87	0	0	133	0	0	0	0
Hf	3.05	1.11	1.13	1.50	6.50	7.37	10.72	3.28	7.97
Ta	1.04	0.12	0.00	0.33	1.66	0.75	1.30	1.21	1.60
Th	11.80	1.42	1.60	1.58	2.37	16.60	25.20	4.10	24.30
Sc	19.8	29.2	21.7	16.8	37.9	12.1	13.6	5.6	0.4
Co	29.7	20.9	0.0	0.0	54.0	0.0	0.0	0.0	0.0
La	43.5	4.6	4.3	5.3	19.5	45.9	52.4	14.3	61.4
Ce	86.1	10.7	9.5	14.3	54.1	89.5	109.8	28.8	133.7
Nd	38.4	7.1	7.9	7.2	37.7	38.3	49.6	16.4	53.0
Sm	6.95	2.00	2.30	2.00	8.68	10.10	13.50	3.80	12.00
Eu	1.84	0.81	0.80	0.68	2.82	1.75	1.49	0.74	0.37
Tb	0.93	0.49	0.50	0.41	1.58	1.24	1.60	0.55	1.97
Ho	0.00	0.67	0.00	0.00	2.38	0.00	0.00	0.00	0.00
Tm	0.32	0.19	0.00	0.00	0.78	0.00	0.00	0.00	0.00
Yb	2.64	1.74	2.00	0.90	3.90	2.60	4.40	1.90	4.20
Lu	0.00	0.28	0.26	0.13	0.57	0.28	0.52	0.22	0.57

Samp.	G250C	Qy175	Qy166	G253L	Qy174	Qy87	Bb107	Bb95	Bb124
Seq.	KD2	KD2	KD2	KT1	KT1	QPg1	TQ2	TQ1	TQ3
Rock	b/a.	b/a.	rhy.	bas.	bas.	tra.	bsn.	phn.	and.
Type	L	L	L	D	D	P	L	L	L
SiO_2	53.60	54.25	72.30	50.40	45.67	59.37	44.90	56.90	57.60
TiO_2	1.03	0.94	0.26	0.98	1.00	0.40	1.24	0.93	1.26
Al_2O_3	18.60	19.20	14.63	15.30	19.81	15.39	12.40	17.40	14.20
Fe_2O_3	9.34	8.10	1.93	9.50	9.11	3.53	8.92	5.68	5.68
MnO	0.17	0.25	0.13	0.19	0.20	0.07	0.16	0.09	0.09
MgO	3.64	4.00	0.40	10.10	6.76	1.60	10.30	1.64	2.82
CaO	7.68	8.80	1.80	10.60	11.31	5.68	12.10	3.38	7.28
Na_2O	2.60	2.23	2.38	1.48	1.93	4.06	3.31	2.58	3.18
K_2O	1.14	0.28	3.62	1.28	1.66	5.33	3.89	7.71	3.68
P_2O_5	0.19	0.22	0.08	0.12	0.22	0.40	1.53	0.83	0.65
LOI	2.62	1.74	5.05	1.06	2.09	2.65	1.91	1.98	1.89
Total	100.61	100.01	102.58	101.01	99.76	98.48	100.66	98.92	98.33
Zr	198	170	158	79	93	203	443	587	516
Y	31	31	9	19	23	10	41	37	20
Nb	9.7	12.0	11.0	6.6	8.0	13.0	27.0	40.0	33.0
Rb	60.0	11.0	163. 0	68.0	113.0	169.0	213.0	217.0	130.0

PHILOSOPHICAL TRANSACTIONS OF THE ROYAL SOCIETY A MATHEMATICAL, PHYSICAL & ENGINEERING SCIENCES

TABLE 1. (*cont.*)

Samp.	G250C	Qy175	Qy166	G253L	Qy174	Qy87	Bb107	Bb95	Bb124
Seq.	KD2	KD2	KD2	KT1	KT1	QPg1	TQ2	TQ1	TQ3
Rock	b/a.	b/a.	rhy.	bas.	bas.	tra.	bsn.	phn.	and.
Type	L	L	L	D	D	P	L	L	L
Sr	259	241	142	208	259	2607	2941	4040	1096
Cr	30	0	0	640	0	0	520	70	61
Ni	9	0	0	125	0	0	148	37	33
V	150	0	0	260	0	0	186	63	75
Cu	17	0	0	40	0	0	47	28	18
Zn	106	0	0	89	0	0	99	101	154
Hf	5.00	4.54	4.20	1.94	2.49	5.40	9.05	12.46	9.65
Ta	0.76	0.29	0.33	0.33	0.84	0.76	1.25	1.82	1.43
Th	8.26	7.40	17.10	1.80	7.00	24.20	89.27	114.16	35.93
Sc	25.7	31.0	5.7	37.6	37.1	7.3	23.3	8.4	8.1
Co	26.3	0.0	0.0	40.7	0.0	0.0	37.9	6.6	8.7
La	21.6	23.7	36.3	8.3	8.3	75.4	325.9	328.4	137.7
Ce	52.3	41.2	57.8	18.6	22.8	139.0	657.8	571.5	275.3
Nd	27.7	21.3	20.0	10.3	12.6	51.3	250.0	204.4	100.5
Sm	5.71	5.60	3.30	2.78	3.80	10.10	33.41	26.01	12.29
Eu	1.59	1.53	0.96	0.83	1.27	1.85	8.38	6.56	2.79
Tb	1.01	0.82	0.37	0.49	0.70	0.57	2.49	1.94	0.93
Ho	1.63	0.00	0.00	0.85	0.00	0.00	0.00	0.00	0.00
Tm	0.42	0.00	0.00	0.19	0.00	0.00	0.00	0.00	0.00
Yb	3.77	1.90	1.00	1.80	2.10	0.90	2.28	2.53	1.35
Lu	0.53	0.28	0.11	0.30	0.30	0.12	0.30	0.34	0.14

Pearce 1984). The patterns drawn depict the range from tholeiitic (OWP1) through alkalic (OWP2 and OWP3) to ultra-alkalic (CWP1). Figure 2*b* shows patterns for four typical continental transitional-to-tholeiitic basalts. Of these, AWP1 and AWP2 also show small and variable degrees of intraplate enrichment: AWP1 is transitional between the oceanic tholeiite pattern (OWP1) and the flat N-MORB pattern; and AWP2 resembles the oceanic tholeiite pattern. By contrast, AWP3 and AWP4 show a small degree of intraplate enrichment on which is superimposed a selective enrichment in large ion lithophile (LIL) elements (Th, La and Ce) which can usually be attributed to crustal assimilation (Thompson *et al.* 1982). The patterns for volcanic arc basalts in figure 2*c* also show selective enrichments in some or all of the LIL elements, in this case due primarily to the metasomatism of the mantle wedge source by aqueous-to-siliceous fluids derived from the subduction zone (see e.g. Pearce 1984). However, it should be noted that subduction and assimilation components cannot be simply distinguished on these plots, and that assimilation can sometimes also be important in these settings: the LIL-enrichment component is therefore termed a subduction/assimilation component in the following text. The degree of LIL element enrichment increases from tholeiitic (OVA1) through calc-alkaline (OVA2 and CVA2) to shoshonitic (CVA1) basalts; basalts erupted in active continental margins (CVA1 and CVA2) and alkaline basalts in island arcs (not shown) can be distinguished from island arc tholeiitic (OVA1) and calc-alkaline (OVA2) basalts by negative slopes of the high field strength (HFS) elements (Nb, Ta, Hf, Zr, Ti, Y and Yb), indicating intraplate as well as subduction/assimilation components. Figure 2*d* illustrates patterns for some post-collision basalts ranging from calc-alkaline (PCL1) through alkalic and shoshonitic (PCL2 and PCL3) to ultrapotassic (PCL4): these most closely resemble patterns from active

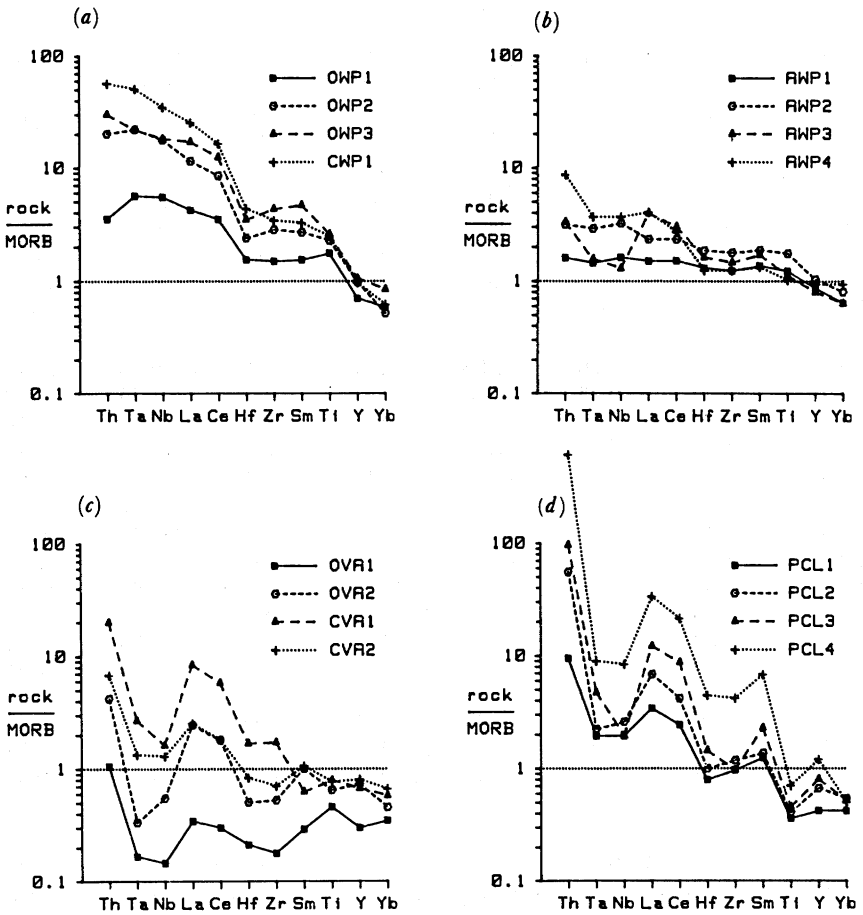

FIGURE 2. Reference MORB-normalized geochemical patterns for basalts of known eruptive environment for comparison with Geotraverse samples in figures 7, 10, 13, 16 and 19. Figure 2*a* shows basalt patterns from oceanic and continental within-plate (OWP and CWP) settings from Loihi, Hawaii (OWP1: Frey & Clague 1983), Ascension and Gough Is. (OWP2 and OWP3: Weaver *et al.* 1987), and Uganda (CWP1: Mitchell & Bell 1976). Figure 2*b* shows basalt patterns from attenuated continental within-plate (AWP) settings from Mull (AWP1: Morrison *et al.* 1980), Skye (AWP2 and AWP3: Thompson *et al.* 1982) and Columbia River (AWP4: Hooper *et al.* 1984). Figure 2*c* shows basalt patterns from oceanic and continental volcanic arc (OVA and CVA) settings from Tonga (OVA1: Ewart *et al.* 1977), New Hebrides (OVA2: Gorton 1977), Chile (CVA1: JAP, unpublished data) and Colombia (CVA2: Marriner & Millward 1984). Figure 2*d* shows basalt patterns from post-collision (PCL) settings from Iran (PCL1: Riou *et al.* 1981), the Alps (PCL2 and PCL4: Venturelli *et al.* 1984), and the Roman province (PCL3: Rogers *et al.* 1985).

continental margin basalts but can occupy all parts of the spectrum from intraplate to continental arc compositions.

The discrimination diagrams utilize the geochemical enrichment patterns shown in the MORB-normalized patterns, but define the boundaries between the various magma types better: thus the Ti–Zr–Y diagram (figure 3*a*) generally indicates the degree of intraplate enrichment, basalts from such sources plotting in the within-plate field on the diagram; and the Th–Ta–Hf diagram (figure 3*b*) generally indicates the degree of subduction zone enrichment, basalts from these sources plotting in the volcanic arc field on this diagram. Since these diagrams were originally published, it has become clear that some ambiguities can occur. Notably: some continental tholeiites may not be derived from sufficiently enriched sources to

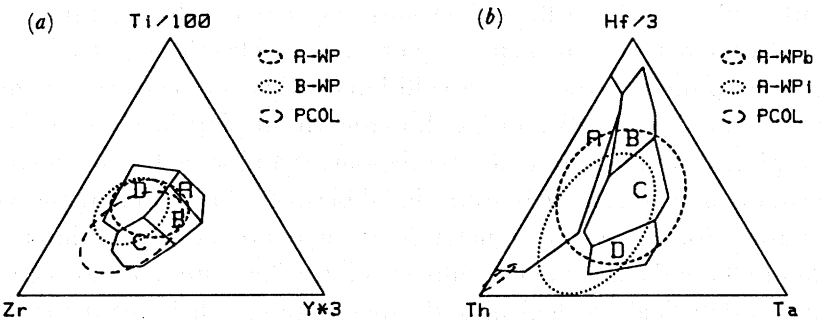

FIGURE 3. Ti–Zr–Y and Th–Ta–Hf discriminant diagrams used to classify Geotraverse basalts, also showing 90% probability ellipses for transitional magma types not considered in original publications. Figure 3*a* shows fields for within-plate basalts (D), mid-ocean ridge basalts (B), island arc tholeiites (A and B) and calc-alkaline basalts (B and C) with additional fields for basalts from normal and back-arc attenuated continental lithosphere (A- and B-WP) and post-collision settings. Figure 3*b* shows fields for volcanic arc basalts (A), mid-ocean ridge basalts (B and C) and within-plate basalts (C and D) with additional fields for basic and intermediate rocks from attenuated continental lithosphere (A-WPb and A-WPi) and for post-collision basalts.

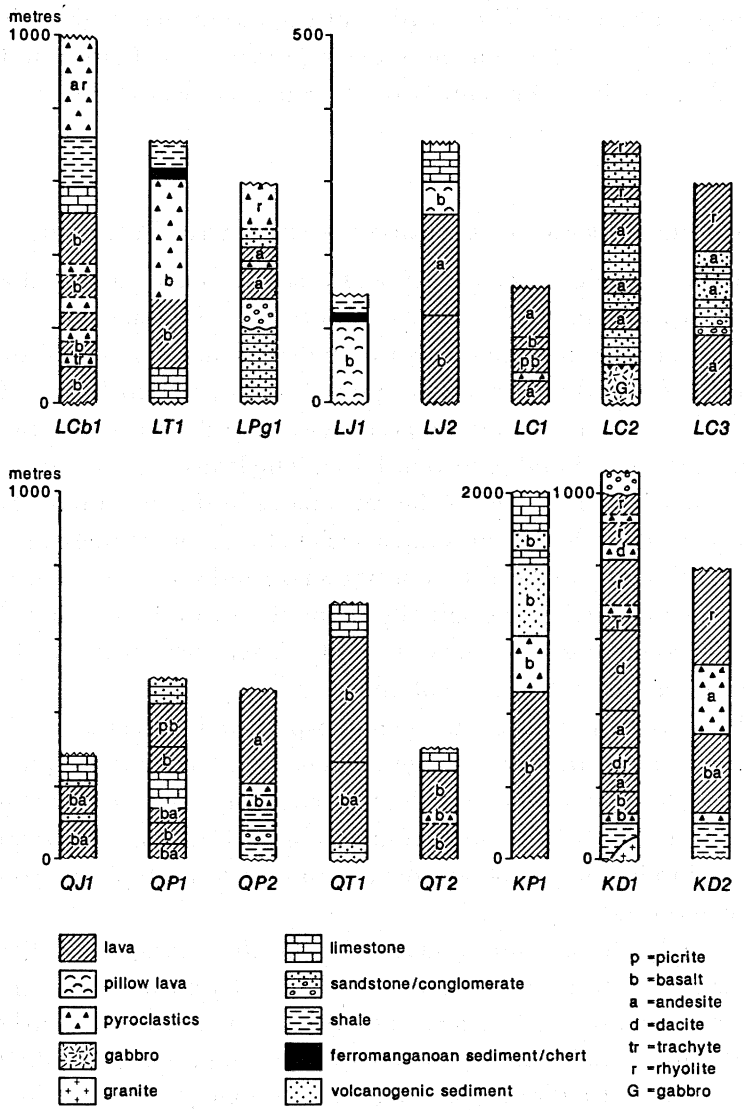

FIGURE 4. Sketch sections showing the volcanic sequences studied during the Geotraverse. For locations, see figures 5, 8, 11 and 14.

plot in the within-plate fields on these diagrams (e.g. Holm 1982); crustal contamination of continental tholeiites may cause them to plot in the volcanic arc field of the Th–Ta–Hf diagram (e.g. Thompson *et al.* 1980); post-collision basalts and some active continental margin basalts may cross from the calc-alkaline basalt to the within-plate field on the Ti–Zr–Y diagram due to the intraplate component in their mantle source; and some basalts, such as ensialic back arc basin volcanics, may be genuinely transitional between the main magma types highlighted in these diagrams. Some additional fields have therefore been superimposed on the two diagrams in figure 3 to take these points into account. Where ambiguities occur, due to basalts plotting in an overlap field, geological and other criteria will be used to try to resolve the ambiguity.

The text that follows considers the geological, petrological and geochemical evidence for the eruptive environments of the various palaeovolcanic provinces encountered during the Geotraverse taken in order from south to north, concluding with a separate discussion of the Tertiary post-collision volcanism and its implications. The volcanic stratigraphy of each sequence studied is recorded in figure 4, although it should be stressed that these were generally mapped at reconnaissance speed. The location of each sequence is given in sketch maps in figures 5, 8, 11, 14 and 18. The sequences are represented in figures and tables by three characters (e.g. LT1), the first representing the terrane, the second the age and the third the location.

3. South Lhasa Terrane (Carboniferous and Triassic) Provinces

Thick sequences of volcanic rocks are exposed east and north-east of Lhasa (figure 5). In their best-exposed area around Dagze they comprise a *ca.* 1500 m-thick sequence of basalt-andesite sheet flows and tuffs (interbedded with mudrocks and limestones) overlain by a thick sequence of ignimbrites and rhyolite flows (figures 4 and 5, section LCb1). In the other area studied, north-east of Maqu, a sequence of basic lavas and tuffs is overlain by ferromanganoan sediments and cherts (figures 4 and 5, section LT1). The lavas overlie and/or are interbedded with platform carbonates in both areas. The carbonates in the north have been dated as late Anisian (Smith & Xu, this volume), and the associated lavas have therefore been taken to be mid-Triassic in age, belonging to the Yeba Formation of southern Tibet (Yin *et al.*, this volume). The southern sequence (LCb1) was originally thought also to be of Triassic age but palynomorphs of late Carboniferous age have recently been identified in shales intercalated within the volcanics (Smith & Xu, this volume).

The basic rocks in both provinces are metamorphosed in greenschist facies to chlorite–epidote–albite–calcite–magnetite assemblages. Phenocrysts, commonly pseudomorphed, are mainly plagioclase with some olivine and clinopyroxene and may comprise up to 50% of the rock. Intermediate and acid rocks are most common in the Carboniferous sequence: the former sometimes also contain phenocrysts of hornblende and the latter typically contain phenocrysts of biotite, feldspar and quartz.

The lavas are strongly altered and so have been classified using the Zr/Ti–Nb/Y diagram (figure 6*a*), both suites plotting within the sub-alkaline basalt and andesite fields (Carboniferous rhyolites are also present but have not been analysed). The Carboniferous basalts exhibit a very slight and variable intraplate component and a major subduction/assimilation component on a MORB-normalized plot (figure 7*a*). They plot within fields B and C

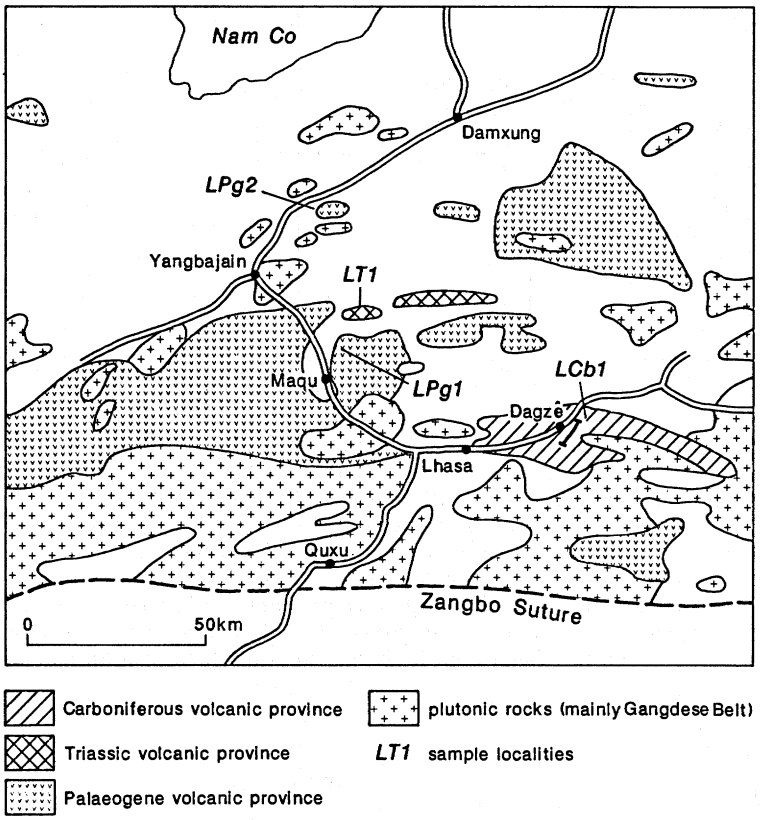

FIGURE 5. Sketch map of the southern part of the Lhasa terrane (see figure 1) showing the approximate known distribution of the volcanic provinces and the locations of the sequences studied.

(calc-alkaline volcanic arc) on the Ti–Zr–Y diagram (figure 7*c*) and in the volcanic arc field on the Th–Ta–Hf diagram (figure 7*d*). The basalts from the Triassic sequence (LT1) have not been fully analysed at the time of writing. However, existing data show that they have similar concentrations of Zr, Y and Nb to the Carboniferous basalts but significantly higher Th concentrations, indicating a similar MORB-normalized pattern shape but with a greater subduction/assimilation component. The two analysed basalts from this sequence plot in the calc-alkaline volcanic arc fields on the Ti–Zr–Y diagram (figure 7*c*) and in the volcanic arc field of the Th–Ta–Hf diagram (figure 7*d*).

Comparison between figure 7*a* and figure 2 shows that the Carboniferous basalts are transitional between the Colombian active continental margin pattern (CVA2) and the New Hebrides pattern (OVA2), but also have some features in common with post-collision basalts; comparison between figures 7*c*, *d* and figure 3 confirms that a volcanic arc origin is most likely but that a post-collision setting is possible. Since the geological evidence indicates a shallow-water submarine environment, possibly associated with carbonate platform break-up (Leeder *et al.*, this volume), an intracontinental post-collision setting can be rejected on geological grounds. However, post-collision rifting to produce an ocean basin, as in the present-day Tyrhennian Sea, remains a possibility. The best interpretation is still, however, that the Carboniferous lavas were erupted in a volcanic arc on transitional crust.

The setting of the Triassic province was probably similar to that of the Carboniferous province: its trace element concentrations are similar, apart from its greater subduction com-

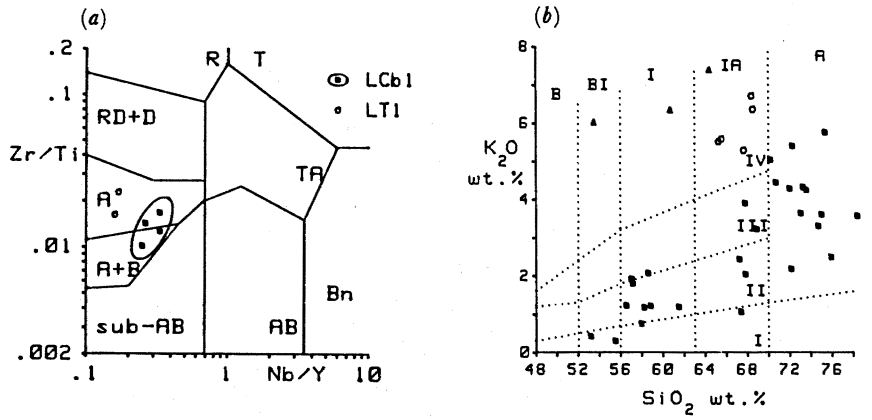

FIGURE 6. (*a*) Zr/Ti–Nb/Y immobile classification diagram and (*b*) K_2O–SiO_2 orogenic rock type classification diagram from South Lhasa Terrane volcanic rocks. In figure 6*a*, the fields shown are for sub-alkaline and alkaline basalts (sub-AB and AB), basalts (B), andesites (A), dacites (D), rhyodacites (RD), rhyolites (R), trachytes (T), trachyandesites (TA) and basanites (Bn). In figure 6*b* vertical boundaries mark the fields for basic (B), basic-intermediate (BI), intermediate (I), intermediate-acid (IA) and acid (A) rocks; boundaries with small positive slopes mark the fields for tholeiitic (I), calc-alkaline (II), high-K calc-alkaline (III) and shoshonitic (IV) series. Also in figure 6*b*, closed squares represent rocks from cycle 1 of the Palaeogene Linzizong Formation (LPg1); open circles represent rocks from cycle 3 of the Linzizong Formation (LPg1); and closed triangles represent rocks from the Yangbajain Basin section of the Linzizong Formation (LPg2).

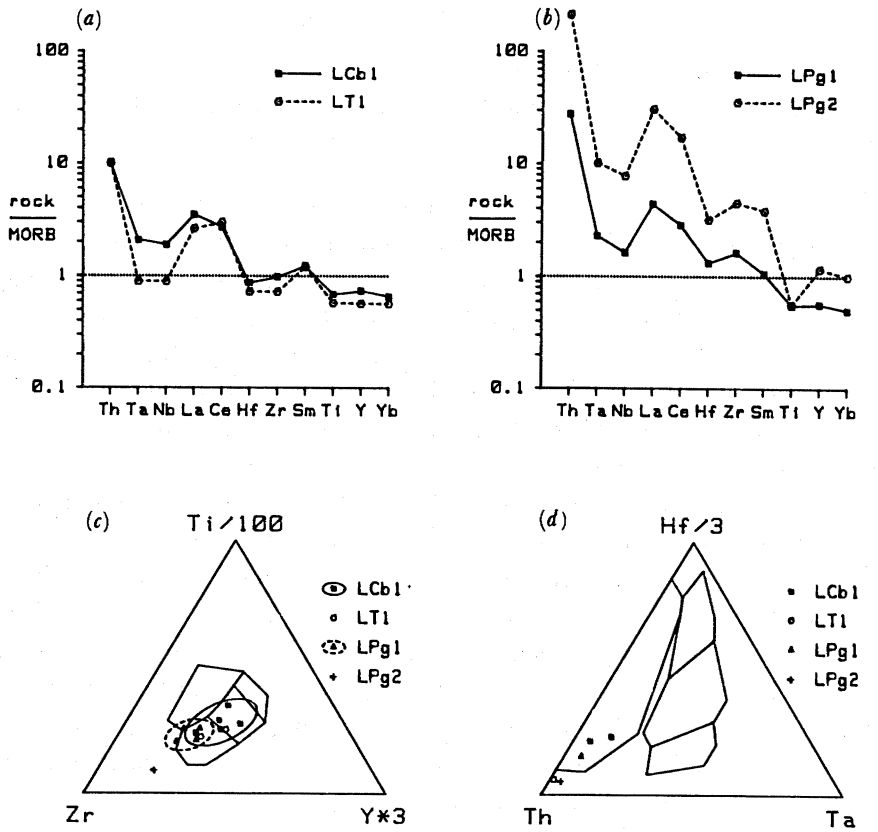

FIGURE 7. (*a*, *b*) MORB-normalized patterns for representative basalts from the Carboniferous (LCb), Triassic (LT) and Palaeogene (LPg) South Lhasa Terrane provinces, and (*c*, *d*) tetonic discrimination diagrams for all basalt samples. Equivalent diagrams for rocks of known setting are given in figures 2 and 3.

PHILOSOPHICAL TRANSACTIONS OF THE ROYAL SOCIETY A MATHEMATICAL, PHYSICAL & ENGINEERING SCIENCES

ponent; and its geologic setting, notably its relationship to carbonate break-up, is comparable. This interpretation is supported by the volcanic arc characteristics indicated by the Ti–Zr–Y and Th–Ta–Hf plots.

4. South Lhasa Terrane (Palaeogene) Province

Palaeogene volcanism is represented in the Geotraverse area by a 1500–2500 m thick sequence known as the Linzizong Formation, which unconformably overlies folded Upper Cretaceous Takena red-beds between Lhasa and Yangbajain and (locally) further north. This sequence has already been studied in some detail (Wang 1980; Coulon *et al.* 1986) and our work was thus confined to a small, confirmatory study.

Wang (1980) described three cycles of volcanism in the Linzizong formation in the area of north of Lhasa. His first cycle consists of a lowermost unit of andesite lavas and pyroclastic rocks and an upper unit of dacitic and rhyolitic pyroclastics, both interbedded with terrestrial clastic sediments and exceeding 1000 m in cumulative thickness. His second cycle is at least 500 m thick and is made up of thick andesite flows. His third cycle is at least 1000 m thick (top not seen) and consists of tuffaceous sandstone overlain by rhyolitic pyroclastics interbedded with tuffaceous sediment and capped by trachydacitic lavas and pyroclastics. Wang also noted a pause in volcanic activity between the second and third cycles. Our own samples were collected from the Maqu region about 40 km north of Lhasa on the east side of the Lhasa-Yangbajain highway in the area of exposure of Wang's first cycle of volcanics (figures 4 and 5, section LPg1). The Linzizong volcanics in this area have given isotopic ages ranging from 60–50 Ma and are locally intruded by the Lhasa granite, which has been dated at about 53 Ma (Xu *et al.* 1985; Coulon *et al.* 1986). A second set of samples was taken a short distance east of the highway some 30 km NE of Yangbajain on the SE flank of the Yangbajain basin, a narrow NE–SW trending graben structure on the SE margin of the Nyainqentanglha range (figure 4, section LPg2). This locality contains a thin sequence of interbedded trachytes and feldspathoid-bearing basalts and was described in some detail by Coulon *et al.* (1986) who dated the sequence as *ca.* 50 Ma by the ^{40}Ar–^{39}Ar technique.

Petrographically the Maqu sequence is strongly porphyritic, containing up to 40% of phenocrysts of plagioclase and some hornblende and clinopyroxene in a cryptocrystalline groundmass. The rocks contain a small number of vesicles and show incipient alteration, notably of hornblende phenocrysts which are pseudomorphed by chlorite and sphene. The rocks north of Yangbajain are quite distinct: the basic rocks contain large euhedral crystals of leucite (pseudomorphed by analcime), plagioclase, titanaugite and olivine in a groundmass of sanidine, aegirine augite and analcime; the trachytes contain large phenocrysts of sanidine and kaersutite in a fine-grained groundmass.

Of the geochemical diagrams, the K_2O–SiO_2 classification plot (figure 6*b*) illustrates Wang's (1980) observation that the rocks become more potassic for a given degree of evolution from bottom to top of the Linzizong sequence, and further emphasizes the ultrapotassic compositions in the Yangbajain Rift. This plot also indicates that crustal assimilation is important in the trend from basic to acid compositions, since the trend is too steep to be accounted for solely by fractional crystallisation. The MORB-normalized plots (figure 7*b*) show strong intraplate and subduction/assimilation components in the basic rocks from both Maqu and, more noticeably, from the Yangbajain rift and resemble the patterns from Chile (CVA1) and the post-collision

localities in figure 2. The Ti–Zr–Y and Th–Ta–Hf diagrams (figures 7*c* and *d*) show characteristics of active continental margin or post-collision basalts for both groups.

Both the geochemistry and the geology of the Linzizong Formation are therefore consistent with the consensus model of an origin above a northward-dipping subduction zone at an active continental margin (e.g. Coulon *et al.* 1986). The strong increase in potassium from cycle 1 to 3 in the lava sequence may indicate the increasing subduction of sediment that accompanied the arrival of a continental margin (in this case the Indian margin), as can be seen at the present-day in Mediterranean arcs and in the Banda arc; alternatively, it could indicate an intra-arc compressional event of the type that has marked the Neogene history of the Central Andes (Bourgois & Janjou 1981). The ultrapotassic compositions in the Yangbajain Rift may also be explained in terms of either an increase in potassium with depth to the Benioff Zone or an origin related to rifting following intra-arc collision.

5. North Lhasa Terrane (Jurassic) Province

Jurassic volcanic rocks have been reported from two major formations within the Lhasa Terrane: the Sangri Group comprising volcanic rocks interbedded with flysch of latest Jurassic to early Cretaceous age from the south of the Terrane; and the Jienong Group, also comprising volcanic rocks interbedded with flysch but of early-to-mid-Jurassic age and from the north of the Terrane around Gyanco (Yin *et al.*, this volume) Neither of these Groups was identified during the Geotraverse, but two sequences of lavas of probable Jurassic age were recognized these are represented as LJ1 and LJ2 in figure 8. Some of these were clearly part of ophiolite complexes and have been discussed in more detail by Pearce & Deng (this volume). Two sequences showed no definite relationship to ophiolites, however, and these are considered here: they are the Loubochong and South Amdo sequences.

The Loubochong sequence (figures 4 and 8, section LJ1) is a 100 m-thick, inverted section of vesicular pillow lavas. The topmost lavas are veined by cherts and these are overlain by cherts and siliceous mudrocks with thin tuff horizons interbedded with cherts. These sediments have been interpreted by Leeder *et al.* (this volume) as representing an oceanic volcano slope. The section south of Amdo (figures 4 and 8, Section LJ2) comprises massive vesicular basalt flows overlain by porphyritic dacite and rhyolite flows, the uppermost of which are pillowed and veined by calcite; these are then overlain by limestone. Geologically this sequence most resembles the upper part of an island arc seamount. To the south and in uncertain relationship with this sequence is a ridge of massive, homogeneous rhyolite.

Petrographically, the Loubochong lavas are strongly metamorphosed to a greenschist facies (chlorite–epidote–calcite–albite) assemblage, are vesicular and either aphyric or clinopyroxene–phyric. The lavas south of Amdo are strongly porphyritic, containing up to 40% by volume of phenocrysts in a cryptocrystalline matrix. The main phenocryst is plagioclase, but clinopyroxene and (in the more basic rocks) olivine are also present. These rocks are also metamorphosed in greenschist facies (albite–chlorite–epidote–calcite) and most phenocrysts are partly or wholly pseudomorphed by alteration phases.

The geochemistry of both sequences is characteristic of island arc tholeiite transitional to island arc calc-alkaline compositions. This is seen, though unreliably due to alteration, in the K_2O–SiO_2 diagram in figure 9. The MORB-normalized patterns in figure 10*a* show low concentrations of the high field-strength (HFS) elements coupled with relative enrichments in the

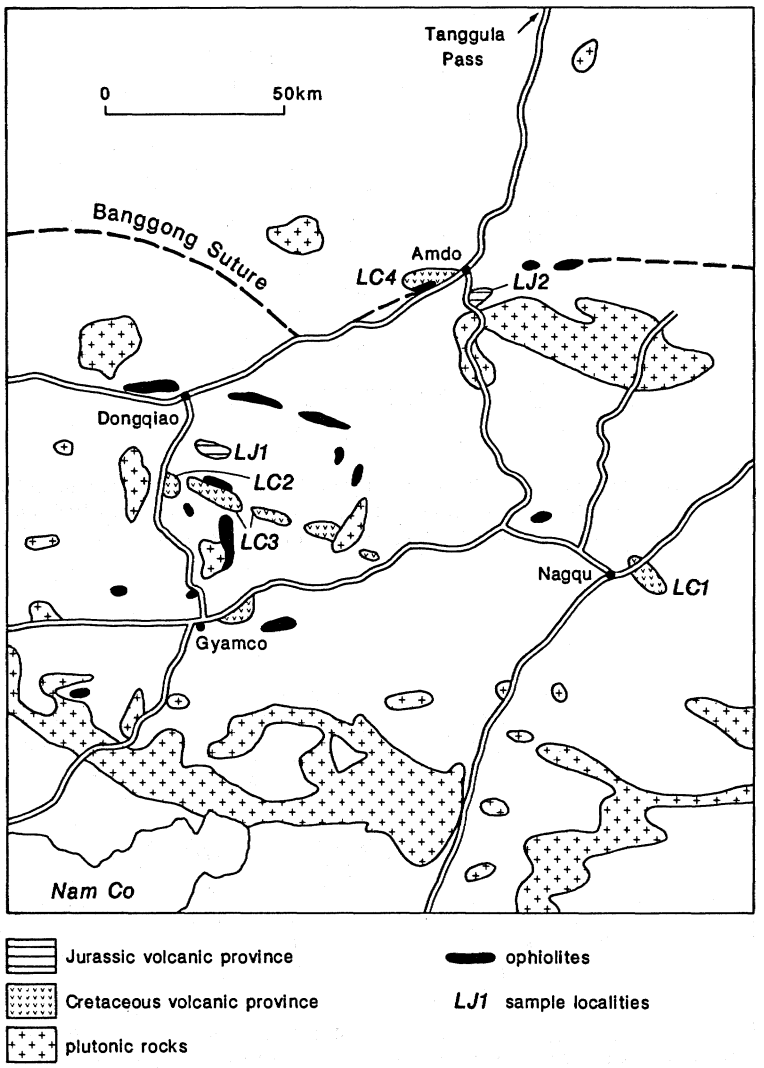

FIGURE 8. Sketch map of the northern part of the Lhasa Terrane showing the approximate known distribution of the volcanic provinces and the locations of the sequences studied.

LIL elements (Th, LREE) and, where not depleted by apatite crystallization, P. Comparison with the 'standard patterns' in figure 2*c* shows strong similarities between both patterns and the patterns for the volcanic arc basalts (OVA1, OVA2 and CVA2). The basic rocks also plot clearly in the volcanic arc fields on the Ti–Zr–Y and Th–Ta–Hf diagrams in figures 10*c* and *d*. A further point of note is that the rhyolite from the ridge south of the South Amdo section is compositionally part of this same province (see data on microfiche 1, in pocket).

Geochemically, therefore, these lavas are of tholeiitic to calc-alkaline island arc composition. Geologically, the lavas south of Amdo probably represent a seamount that approached sea level and accumulated a limestone cover on isostatic subsidence. The rhyolite ridge may also represent some positive submarine topographic feature of the type seen in many recent arc-basin complexes. The Loubochong pillow lavas may represent the flanks of a submarine arc volcano, although they could also have formed at a supra-subduction zone spreading centre: their vesicularity favours the former hypothesis, though not unambiguously. It is probable,

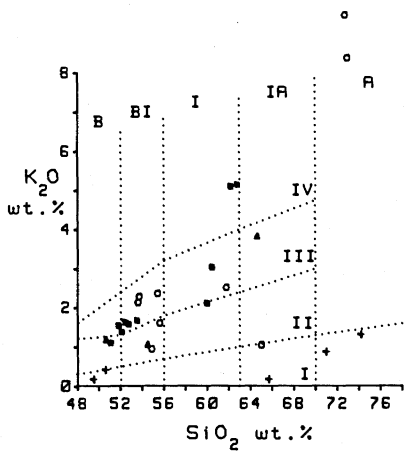

FIGURE 9. K_2O–SiO_2 orogenic rock type classification diagram for North Lhasa Terrane volcanic rocks. Fields are as given in the caption to figure 6. Crosses represent Jurassic volcanics (LJ1 and LJ2 in figure 8); closed squares, open circles and closed triangles represent Cretaceous volcanics from localities LC1, LC2 and LC4 (see figure 8) respectively.

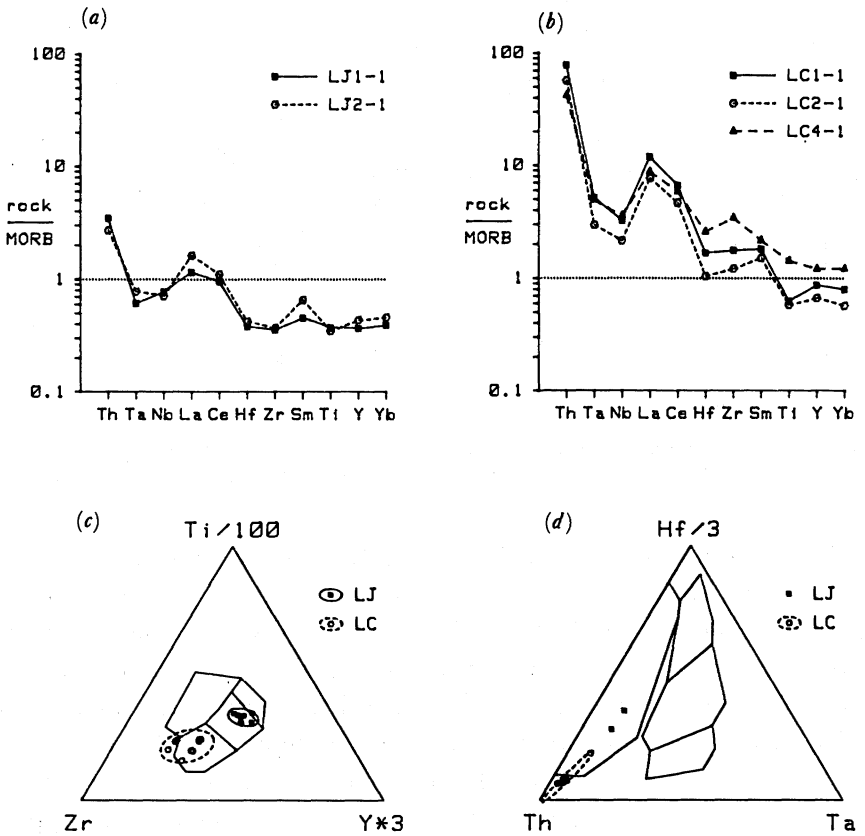

FIGURE 10. (*a*, *b*) MORB-normalized patterns for representative basalts from the Jurassic (LJ) and Cretaceous (LC) North Lhasa Terrane provinces, and (*c*, *d*) tectonic discrimination diagrams for all basalt samples. Equivalent diagrams for rocks of known setting are given in figures 2 and 3.

PHILOSOPHICAL TRANSACTIONS OF THE ROYAL SOCIETY A MATHEMATICAL, PHYSICAL & ENGINEERING SCIENCES

therefore, that the Jurassic volcanics, together with the ophiolite complexes discussed by Pearce & Deng (this volume), formed in various parts of an arc-basin complex. Although more outcrops need to be examined to reach a definite conclusion, the volcanics studied here could represent an island arc separating a fore-arc terrane in the south from a back-arc terrane in the north-dipping subduction zone.

6. North Lhasa and South Qiangtang (Mid-Cretaceous) Province

As noted by other authors, notably Coulon *et al.* (1986), a major calc-alkaline province was active during the period *ca.* 110–75 Ma over a wide region of the Geotraverse area from Nam Co lake in the South to Amdo and perhaps as far as the Tanggula pass in the north (figure 1). Several sections were studied. The *Nagqu section* (figures 4 and 8, section LC1) is primarily made up of columnar-jointed, vesicular, plagioclase-phyric andesites interbedded with basalts, rare volcanic breccias and red-beds which unconformably overlie Middle–Upper Jurassic mudrocks and flysch. A similar sequence from the Nagqu area has been dated tentatively by the ^{40}Ar–^{39}Ar technique as between 100 and 95 Ma (Coulon *et al.* 1986). The *Norbuzhong and Pung Co sections* (figures 4 and 8, sections LC2 and LC3) north of Gyanco comprise a series of andesite and rhyolite flows interbedded with tuffs and red-beds, in the former case unconformably overlying a fragment of the Dongqiao ophiolite. Parts of this sequence have been dated by Coulon *et al.* (1986) as 95–85 Ma. The *Amdo section* (figure 8, section LC4) is an inverted sequence of ophiolitic gabbro overlain unconformably by basaltic andesite to andesite flows and pyroclastic rocks and overthrust by Cretaceous red-beds. This section has been dated by Coulon *et al.* (1986) as between 80 and 76 Ma. In addition to these sections, lavas, flows, pyroclastic rocks and hypabyssal intrusions of andesite to rhyolite composition are found throughout this area and, by virtue of their similar geological setting are assumed to be of similar age. The northernmost occurrence found during the Geotraverse may be a porphyritic rhyolite stock which intrudes Jurassic shales on the south slope of the Tanggula pass; the southernmost may be a series of rhyolite dykes that cut Carboniferous sediments south of Damxung. High-level plutonic equivalents of many of these volcanic sequences also occur, particularly north of Gyanco.

The petrology of the analysed rocks is broadly similar across the province. Virtually all rocks are porphyritic, containing up to 50% by volume of phenocrysts. Plagioclase is the most common phenocryst throughout the fractionation sequence, but mafic phases are also abundant in the more basic rocks. Olivine, clinopyroxene and magnetite are the most common of these, but hornblende and orthopyroxene are present in some samples. Biotite occurs, together with sanidine, in the more evolved rocks. Some intermediate lavas have trachytic textures. Alteration is variable and generally of sericite–chlorite hydrothermal facies: some sericitization of plagioclase is common; hornblende and orthopyroxene have usually experienced partial or total replacement by chlorite and/or calcite and oxides; clinopyroxene can be carbonated; and biotite is commonly oxidized.

The rocks analysed typically plot in the high-K calc-alkaline series fields of the K_2O–SiO_2 diagram (figure 9). MORB-normalized plots (figure 10*b*) show small intraplate and large subduction/assimilation components for basic rocks from all four sections, resembling the patterns from Chile (CVA1) and the post-collision settings in figure 2. The rocks plot on the volcanic arc (calc-alkaline) - within-plate boundary on the Ti–Zr–Y diagram (figure 10*c*) and

within the volcanic arc field of the Th–Ta–Hf diagram (figure 10*d*), indicating an active continental margin or post-collision setting (see figures 2 and 3).

The combination of geochemistry and geology does not totally resolve the ambiguity between an active continental margin and a post-collision origin. Coulon *et al.* (1986) favoured an origin above a shallow N-dipping subduction zone. They considered a post-collision origin, but argued against it, largely on the grounds that the time interval between the collision in the Banggong Suture Zone was too great for collision and volcanism to have been related. We, however, prefer the post-collision hypothesis on the following grounds: the final collision event could have been as late as the age of intrusion of the Baingoin granitoid belt (*ca.* 130–120 Ma: Harris, Xu, Lewis, Hawkesworth & Zhang, this volume), in which case the time interval between collision and the start of postulated post-collision volcanism would lie between 40 and 30 Ma which is roughly the same period as in Tibet and the Alps; the distance from a trench at the southern margin of the Lhasa Terrane would mean an arc-trench gap of 2–500 km, which is unrealistically large by present-day analogies; there is no major difference in composition between the lavas north of Amdo and those near Nagqu, some 150 km to the south, whereas most active continental margins show major space-time geochemical variations. Clearly, however, the closure of the Banggong Suture was such a complex and poorly-understood event that neither possibility can entirely be ruled out.

7. Qiangtang (Jurassic) Province

A sequence of mainly basic Jurassic volcanic rocks at or near the base of the predominantly sedimentary Yanshiping Group was briefly studied north of Wenquan Station (figures 4 and 11, section QJ1). The sequence comprises reddish-brown massive flows intercalated with and overlain by ferromanganoan sediments and is overlain by a yellow limestone and finally by a thick fluviatile sequence which contains marine incursions dated as mid-Jurassic (Smith & Xu, this volume). The volcanics are therefore considered to be of early mid-Jurassic age.

The lavas mainly contain up to 20% of olivine or olivine and plagioclase phenocrysts in a groundmass of plagioclase, clinopyroxene and magnetite. The samples studied have experienced pervasive oxidative alteration in which olivine phenocrysts were altered to mixtures of iddingsite, smectite and calcite, plagioclase phenocrysts were partially altered to clay minerals and the groundmass has been partly replaced by calcite and clay minerals.

The geochemistry of the rocks is also marked by erratic variations in the abundances of alkali elements due to mobility during alteration. On the Ti/Zr–Nb/Y diagram (figure 12*b*), the rocks classify as sub-alkaline andesites. The MORB-normalized patterns (figure 13*a*) show a strong intraplate component and an additional subduction/assimilation component most resembling the Columbia River basalt pattern (AWP4) in figure 2. The analysed samples plot from the volcanic arc/within-plate boundary into the within-plate field of the Ti–Zr–Y diagram (figure 13*d*) and in the volcanic arc field of the Th–Ta–Hf diagram (figure 13*e*). These results indicate an intraplate origin on attenuated lithosphere, either at a passive margin or in a back-arc ensialic setting: a post-collision setting or active continental margin is a possible, but less likely, interpretation.

The apparently minor extent and geologic setting of this sequence argue against an origin at an active continental margin and for an origin on attenuated continental lithosphere, but

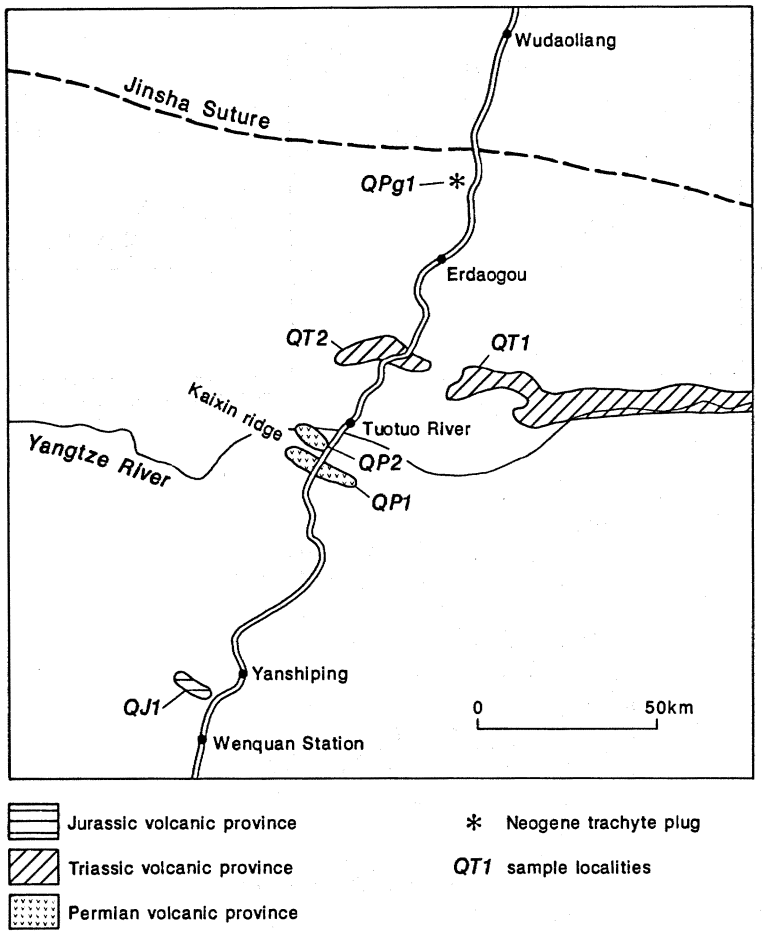

FIGURE 11. Sketch map of the Qiangtang Terrane showing the approximate known distribution of the volcanic provinces and the locations of the sequences studied.

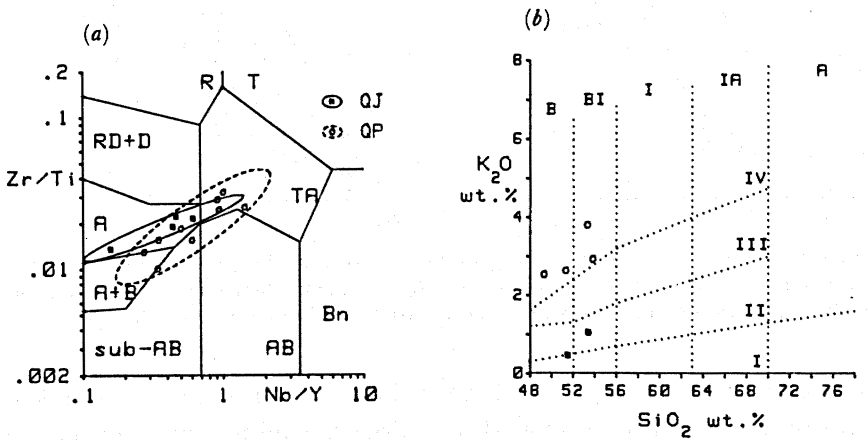

FIGURE 12. (*a*) Zr/Ti–Nb/Y immobile element classification diagram and (*b*) K_2O–SiO_2 orogenic classification diagram for Qiangtang Terrane volcanic rocks. The fields are as given in the caption to figure 6. In figure 12*b*, the closed squares and open circles represent the lower and upper lavas respectively from locality QT1 (figure 11).

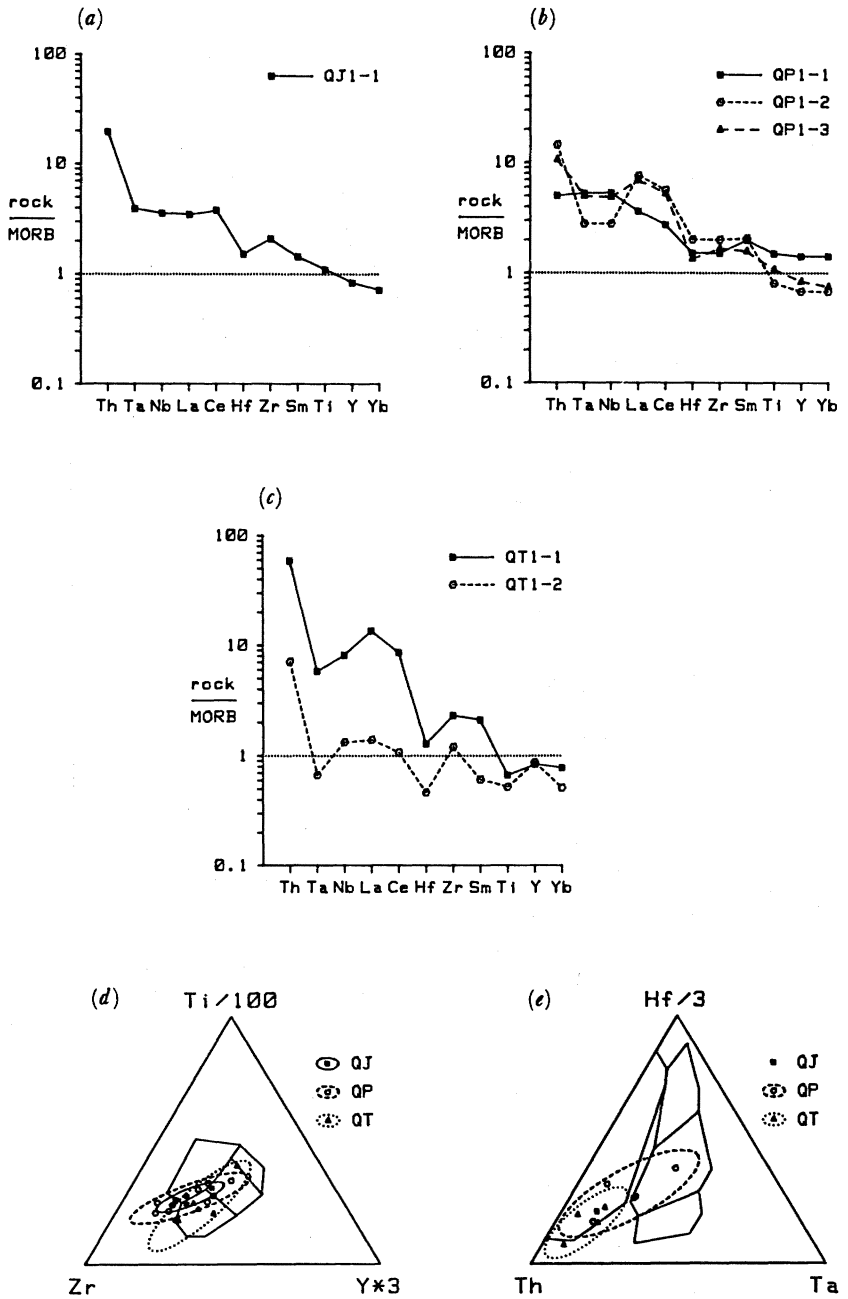

FIGURE 13. (*a–c*) MORB-normalized patterns for representative basalts from the Jurassic (QJ), Permian (QP) and Triassic (QT) provinces, in the Qiangtang Terrane and (*d*, *e*) tectonic discrimination diagrams for all basalt samples. Equivalent diagrams for rocks of known setting are given in figures 2 and 3.

it is not entirely clear whether the eruptive event is best thought of as having taken place in a post-collision rift in a foreland basin related to a Triassic collision event in the north, or at the edge of a marginal basin related to a Jurassic subduction event to the south. Some of the best analogues of both the geology and the geochemistry are found in the trap basalts of Eastern China, on the margin of the Japan and South China Seas (Zhou & Armstrong 1982).

8. Qiangtang (Permian) Province

Lavas from this province were studied during the Geotraverse on and around the Kaixin Ridge, a short distance south of Tuotuohe (figure 11). As explained by Smith & Xu (this volume), the volcanic sequence conformably overlies limestones of early late Permian age and is thus assumed itself to be of late Permian age, correlating with volcanics of the Qamdo region further to the east.

Two sequences were studied, one on the south slope of the Kaixin Ridge (figures 4 and 11, section QP1), the other on the Banacomu Ridge (figures 4 and 11, section QP2). The former is divided into two units separated by a limestone bed. The lower unit is at least 100 m in thickness and comprises (from bottom to top) a basaltic andesite, a dolerite and an andesite unit. The upper unit is about 165 m in thickness and can be divided into a dolerite, a basalt and a picrite basalt unit. The sequence on the Banacomu Ridge begins with variegated red-green mudrocks of assumed continental derivation overlain by about 350 m of volcanic rocks, comprising agglomerate with basalt clasts and a flow-banded andesite. These are overlain by 40 m of coal-bearing clastics with marine bands dated as late Permian (Leeder *et al.*, this volume).

The volcanic rocks are slightly vesicular and generally contain $< 5\%$ of microphenocrysts of plagioclase, and sometimes also olivine and clinopyroxene, in a groundmass of plagioclase, clinopyroxene and magnetite. The picrite, however, contains about 25% of olivine phenocrysts. The rocks have experienced a variable degree of carbonation and clay mineral alteration of phenocrysts and groundmass, and vesicles have been filled with chlorite and calcite. On the immobile element classification diagram, Ti/Zr–Nb/Y (figure 12*a*), the rocks can be seen to be transitional between tholeiitic and alkalic in composition and to range from basalts to andesites and trachyandesites. On the MORB-normalized plots (figure 13*b*), the lavas show a range of patterns. One sample (QP1-1) shows a typical intraplate pattern with no subduction/assimilation component; the others exhibit both an intraplate component and a subduction/assimilation component. On the Ti–Zr–Y diagram (figure 13*d*), the samples plot in the within-plate field, but on the Th–Ta–Hf diagram (figure 13*e*) they form a field spanning the ocean ridge/within-plate and the volcanic arc field. This spectrum of compositions is not seen in volcanic arcs, but is common in lavas erupted in intracontinental rifts on attenuated continental lithosphere where variable crustal assimilation has taken place; samples contaminated by the crust show selective enrichment in LIL elements on a MORB-normalized plot (cf. patterns AWP3 and AWP4 in figure 2*b*) and plot in the arc field on the Th–Ta–Hf diagram, whereas uncontaminated samples have intraplate-MORB patterns (cf. patterns AWP1 and AWP2 in figure 2*b*) and plot in the intraplate-MORB fields on discrimination diagrams (see also Thompson *et al.* 1982). The strong degree of iron-enrichment in some samples from this province (see Appendix, microfiche 1, in pocket) also supports this interpretation.

The geochemical interpretation of an origin within attenuated continental lithosphere during rifting can be put forward with confidence since no other environment shows this type of intrasequence variation. Moreover, the shallow-water geological setting and the abundance of sheet-flows are both consistent with this interpretation.

9. North Qiangtang (Triassic) Province

A major volcanic formation, the Batang Group, crops out mainly to the east of the traverse area in the Qiangtang Terrane. Although not of the thickness described for the Batang Group in its type area, lavas assumed to belong to this group were identified east and west of the highway between Tuotuohe and Erdaogou (figure 11). In the eastern section, at Zhakongjian (figures 4 and 11, section QT1), a *ca.* 500 m thick sequence of basalt–andesite lavas flows overlies a fluvial sequence of conglomerates and sandstones and is directly overlain by marine carbonates and clastics (Leeder *et al.*, this volume). The limestones have been given a Norian age by Smith

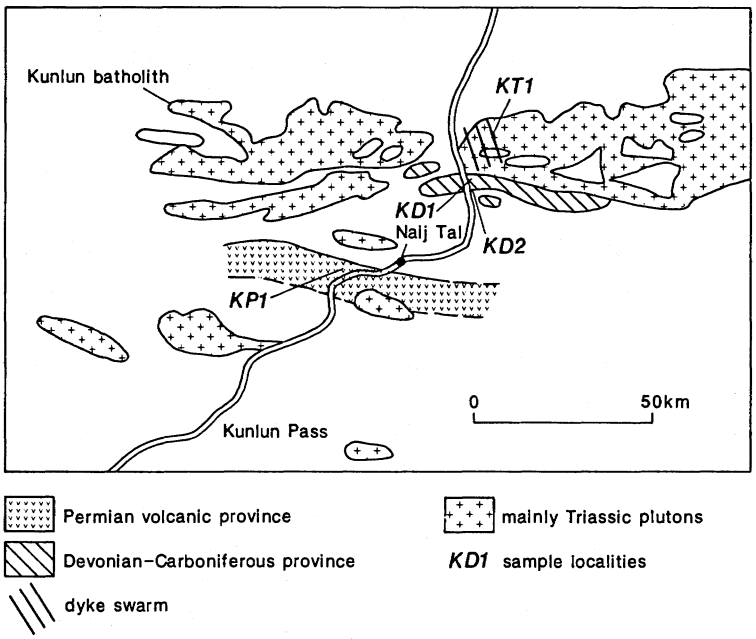

Figure 14. Sketch map of the Kunlun Terrane showing the approximate known distribution of the volcanic provinces and the locations of the sequences studied.

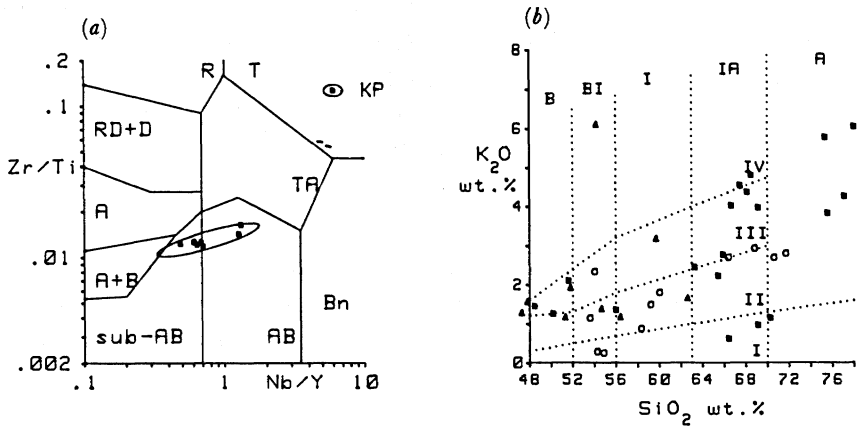

Figure 15. (*a*) Zr/Ti–Nb/Y immobile element classification diagram and (*b*) K_2O–SiO_2 orogenic classification diagram for Kunlun Terrane volcanic rocks. Fields are as given in the caption to figure 6. The closed squares and open circles represent localities KD1 and KD2 (see figure 14) respectively; the closed triangles represent locality KT1.

& Xu (this volume), suggesting that the volcanics are early late Triassic in age. This sequence has been divided into a lower and an upper lava unit on the basis of geochemistry as explained below. The lava flows have a general E–W strike and dip steeply south. In the western section (figures 4 and 11, section QT2), near the 85th Highway Maintenance Squad on the Golmud highway, a *ca.* 130 m sequence of basalt–andesite lava flows and agglomerates (base not seen) is also overlain by a limestone of probable Norian age (Smith & Xu, this volume) and is thus assumed to belong to the same volcanic province. These lavas also strike approximately E–W but dip north at about 45°.

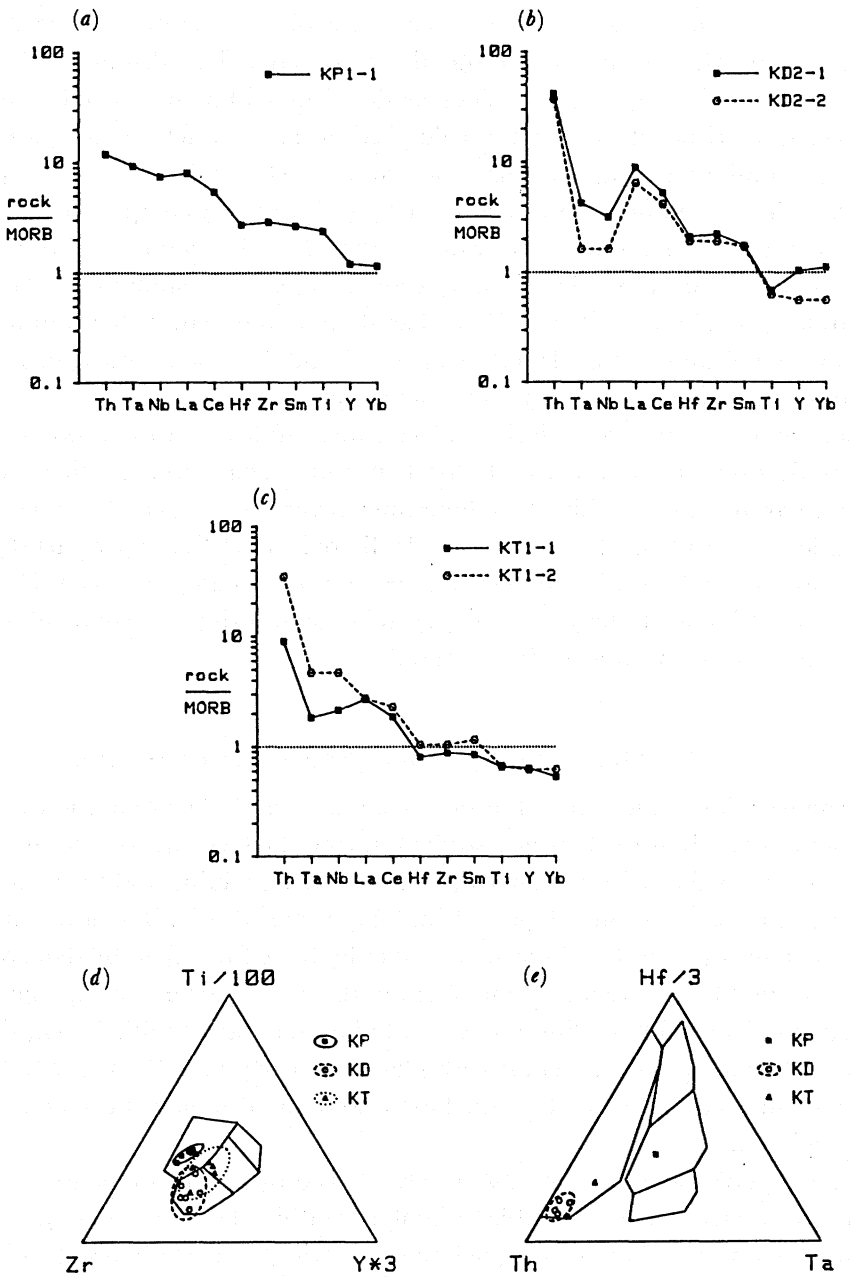

FIGURE 16. (*a–c*) MORB-normalized patterns for representative basalts from the Permian (KP), Devonian/Lower Carboniferous (KD) and Triassic (KT) provinces in the Kunlun Terrane and (*d*, *e*) tectonic discrimination diagrams for all basalt samples. Equivalent diagrams for rocks of known setting are given in figures 2 and 3.

Petrographically, the lavas are all strongly porphyritic, typically containing 30–50% of phenocrysts of olivine, plagioclase and clinopyroxene in a cryptocrystalline matrix. The dominant phenocryst is plagioclase, except in the upper unit from QT1 where the three minerals are in approximately equal proportions. The lavas all exhibit evidence of a moderate degree of low-temperature alteration: olivine is usually partly altered to combinations of iddingsite, serpentine, green and brown smectite and calcite, plagioclase to clay minerals and pyroxene to calcite; brown smectite and calcite are abundant in the groundmass.

Geochemically, the lavas fall into two groups. On the K_2O–SiO_2 diagram (figure 12*b*), the western lavas and the basal group of the eastern lavas plot as members of the calc-alkaline series; whereas the upper group of the eastern lavas plot as members of the shoshonitic series, having very high primary contents of the alkali elements. This distinction is also seen in the MORB-normalized plots (figure 13*c*). Whereas the calc-alkaline basalt of the former group has a pattern characteristic of an oceanic calc-alkaline arc, namely a flat pattern on which a subduction/assimilation component is superimposed (cf. the New Hebrides pattern, OVA2, in figure 2*c*), the shoshonitic basalt shows a large intraplate component as well as the subduction/assimilation component. In view of the close association of these two lavas, the shoshonitic pattern must represent an oceanic alkali arc pattern similar to that of Grenada in the Lesser Antilles (not shown in figure 2), rather than a continental shoshonite. Both groups of lava plot in the volcanic arc fields of the Ti–Zr–Y and Th–Ta–Hf diagrams (figures 13*d* and *e*), thus confirming their volcanic arc characteristics.

The rocks analysed are characteristic of volcanic arc lavas erupted on oceanic or thinned continental lithosphere in terms of both their mineralogy and geochemistry. Their local geological environment, notably their limestone cover, also suggests submarine edifices that have isostatically subsided. The presence of alkali arc lavas in the upper part of the eastern lava sequence may, by analogy with similar compositions elsewhere, such as in Grenada and some of the Aleutian Islands (Delong *et al.* 1975) indicate an origin above a subducted transform fault or close to an arc-transform intersection.

10. Central Kunlun (Permian) Province

This province is known to extend for some distance in an E–W orientation within the Central Kunlun mountains (figure 14). It was studied during the Geotraverse within and to the south of the Wanbaogou valley east of Naij Tal. Despite intense folding and thrusting, it was possible to recognize some stratigraphy (figures 4 and 14, section KP1). The lower unit comprises at least 1.5 km of massive basalts; these are overlain by basic tuffs, then by redeposited tuffs. Thin limestone (marble) bands are intercalated within the upper part of the sequence, which appears to be overlain conformably by limestones of late Permian age (Smith & Xu, this volume); the age of the volcanic episode is tentatively placed at early-mid Permian. Sills within Lower Palaeozoic strata south of the area studied are also thought to have been emplaced during this magmatic episode.

The original petrology of the lavas is largely masked by regional metamorphism: most rocks exhibit a greenschist facies assemblage (chlorite–albite–epidote–calcite), but this rises to amphibolite facies (hornblende–plagioclase–magnetite ± epidote ± zoisite ± calcite) in thrust zones.

The immobile Ti/Zr–Nb/Y classification diagram (figure 15*a*) shows the lavas to be

predominantly basaltic and to be transitional between tholeiitic and alkalic in composition. The MORB-normalized pattern (figure 16*a*) is typical of a transitional intraplate basalt lacking any subduction/assimilation component (c.f. OWP1 in figure 2*a*). This interpretation is supported by the Ti–Zr–Y (figure 16*c*) and Th–Ta–Hf (figure 16*d*) diagrams, both of which show all the analysed samples to have typical intraplate character.

Geochemical evidence is equally consistent with an origin in a continental rift during moderate lithospheric attentuation or in a major oceanic plateau or island chain. Geological evidence, notably the presence of sills within continental basement and the absence of any pillowed flows in the lower part of the sequence favours the continental rift hypothesis.

11. North Kunlun (Devonian/Carboniferous) Province

Volcanic rocks outcrop along the Dagangou valley for about 10 km south of the Kunlun batholith (figure 14); these are thought to be part of a major linear province that extends E–W for thousands of kilometres along the northern part of the Kunlun range. The area studied contains two volcanic formations, one to the north and one to the south, separated by an E–W valley in which there is no exposure. The northern formation (figures 4 and 14, section KD1) strikes consistently at 060° and has a constant 40° SE dip; the southern formation (figures 4 and 14, section KD2) has a similar strike but is gently folded. The 1982 reconnaissance map (Academia Sinica, unpublished data) shows the northern outcrop as 'Devonian' and the southern outcrop as 'Carboniferous'. However, the age of neither formation is completely certain. Both formations are underlain by mudrocks and siltstones of unknown age. The northern formation is intruded and contact metamorphosed by the Triassic Kunlun batholith (Harris, Xu, Lewis & Jin, this volume) and both formations are cut by minor intrusions that are assumed to be of similar age to the batholith. The northern formation is overlain by a thick sequence of conglomerates and arkosic sandstones, a similar sequence to that overlain elsewhere by a fossiliferous sequence of late Visean/early Namurian fluvio-deltaic sediments (Smith & Xu, this volume) and is therefore probably of pre-mid-Carboniferous age. The southern formation was always observed to be in fault contact with these sediments and is therefore of uncertain age. For the purposes of this paper, a Devonian/early Carboniferous age will be assumed for both formations.

Interpretation of the volcanic stratigraphy is complicated by the presence of late Triassic dykes and sills (described in the next section) which cut the volcanic rocks, the Kunlun batholith and the Carboniferous sediments and which have a similar mineralogy and chemical signature to the lavas. Our tentative stratigraphic interpretation shows the northern formation to have an agglomerate at its base, overlain by several units of basalts, andesites and rhyolites; it has a total thickness of *ca.* 900 m. The southern formation also has an andesitic agglomerate at its base overlain by an andesitic and a rhyolitic unit reaching a total thickness (top not seen) *ca.* 700 m.

The mineralogy of the lavas is typically orogenic. The basic-intermediate rocks are porphyritic, containing up to 50% phenocrysts, mainly of plagioclase, and also of hornblende and magnetite. The acid rocks are also highly porphyritic, containing phenocrysts of K-feldspar, plagioclase, hornblende, biotite and, sometimes, resorbed quartz. All rocks have been strongly altered by hydrothermal processes which were probably associated with the intrusion of the Kunlun batholith. Close to the batholith itself, the lavas have experienced a K-silicate

PHILOSOPHICAL TRANSACTIONS OF THE ROYAL SOCIETY A MATHEMATICAL, PHYSICAL & ENGINEERING SCIENCES

alteration in which hornblende was pseudomorphed by clusters of biotite and the groundmass largely replaced by tiny biotite grains and secondary quartz. Further from the intrusion, alteration was of propylitic type, in which hornblende was pseudomorphed by clusters of chlorite and magnetite, plagioclase phenocrysts sometimes partly pseudomorphed by epidote and the groundmass converted to an assemblage of sericite, chlorite and secondary quartz. Superimposed sericitic and argillic alteration has altered most feldspar phenocrysts to a mixture of sericite and kaolinite.

Geochemical classification by the K_2O–SiO_2 diagram (figure 15*b*) is not reliable owing to metasomatic effects, by which potassium has been introduced during K-silicate, and removed during propylitic, alteration. However, taking these effects into account, the diagram does indicate that the lavas all belong to the calc-alkaline or high-K calc-alkaline series. The MORB-normalized plots (figure 16*b*) for the most basic lavas reveal a combination of intraplate and subduction/assimilation components typical of active continental margins, some ensialic back-arc rifts and post-collision settings. The Ti–Zr–Y (figure 16*d*) and Th–Ta–Hf (figure 16*e*) discrimination diagrams also show distributions of data points characteristic of these environments. The relationship between the low- and high-K calc-alkaline series can best be represented on plots of more petrogenetic significance. The chondrite-normalized REE plot (figure 17*a*), shows how a parent basalt (Qy175) evolves towards acid compositions. Evolution of the low-K calc-alkaline series towards rhyolites (e.g. Qy166) is accompanied by a slight enrichment in light REE and depletion in heavy REE , a characteristic of significant amphibole fractionation. By contrast, evolution of the high-K calc-alkaline series towards andesites (e.g. Qy171) and rhyolites (e.g. Qy206) is marked by enrichment in both light and heavy REE, giving a somewhat flatter pattern, a feature characteristic of crystallization of anhydrous phases (olivine, plagioclase, pyroxenes and magnetite) throughout. Such a contrast in crystallization behaviour may indicate a change in source region. It can happen during the evolution of active continental margins, but, perhaps significantly, is also characteristic of a change from subduction to collision environment, as for example during Neogene volcanism in Eastern Anatolia (Yilmaz *et al.*, 1987).

Geochemically and geologically, the lavas from this province could have an active continental margin or a post-collision origin, or both. The geochemical argument presented above

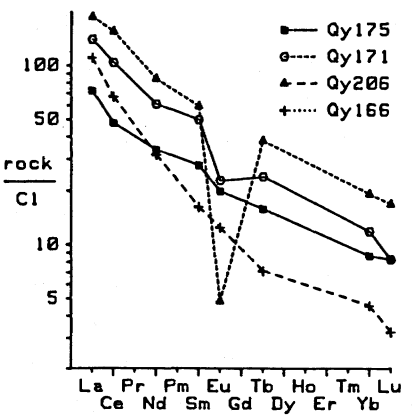

FIGURE 17. Chondrite-normalized REE plot for lavas from the Devonian/Lower Carboniferous province in the Kunlun Terrane: for full analyses see table 1.

gives the lower lava units a greater probability of an origin in an active continental margin, and the upper unit a greater probability of an origin in a post-collision setting, but a final interpretation must await further work on the geology and volcanic evolution of the province.

12. North Kunlun (Permo–Triassic) Province

There are no obvious eruptive products of this province, which is represented in the traverse area by swarms of basalt–andesite dykes which cut the Kunlun batholith and adjacent terrain and by sills of similar composition which cut the Carboniferous sedimentary strata and, as indicated above, the Devonian/Lower Carboniferous volcanic sequences (figure 14, locality KT1). Given the likely age of between 260 and 240 Ma for the Kunlun batholith (Harris, Xu, Lewis, Hawkesworth & Zhang, this volume), the dykes can be assigned an age of post-late Permian. The nature of dyke alteration (discussed below) further indicates that the dykes were intruded before the batholith had cooled; if so, the dykes can be assigned a probable late Permian to early Triassic age. The dyke swarm varies in intensity within the study area, reaching a maximum 10% of the outcrop in the area shown in figure 14. A brief study indicated two major dyke orientations, the dominant trend being NW–SE with a dip of 75° NE, the subsidiary trend being N–S and vertical.

Texturally, the dykes and sills have equigranular, ophitic textures, and this serves to distinguish them from the porphyritic lavas within the Devonian/Lower Carboniferous terrain. Typically, feldspar laths have been sericitized and poikilitic clinopyroxenes altered to actinolite and biotite. This similarity in hydrothermal alteration assemblages between the Triassic dykes and the Palaeozoic lavas suggests that both were altered at the same time; the zonation of alteration around the batholith in both dykes and lavas suggests that the batholith was the heat source for the hydrothermal alteration: the net conclusion is, therefore, that the dykes were intruded into the batholith while it was still hot enough to set up hydrothermal circulation.

Geochemically, the dykes analysed are dominantly calc-alkaline basaltic andesites and andesites, plotting in the same fields as the Devonian/Lower Carboniferous rocks of similar silica content in the discrimination diagrams of figures 16*c* and *d*. They could also be interpreted equally as active continental margin or post-collision intrusions. The major exception is sample G253Y, which is characterized by high concentrations of HFS elements, most notably Zr, which exceeds 1500 p.p.m. This composition is characteristic only of post-collision settings, but its age is not well-defined since it cuts sediment near the granite contact rather than the granite itself.

Despite the ambiguity in the tectonic interpretation of the dyke geochemistry, geological and isotopic evidence from the Kunlun granitoids (Harris, Xu, Lewis, Hawkesworth & Zhang, this volume) suggests that the 260–240 Ma Kunlun batholith pre-dated collision and that the belt of granitoids south of Naij Tal, dated at 200–190 Ma, post-dated collision. If the dykes are broadly contemporaneous with the Kunlun batholith, they must therefore also pre-date collision and be of active continental margin origin.

13. Oligocene–Recent post-collision volcanism

Although little is known about the timing and distribution of magmatism following the start of India–Eurasia collision in the Palaeogene, three distinct post-collision volcanic provinces can be identified (figure 18). The earliest of these, evidence of which was encountered during the

PHILOSOPHICAL TRANSACTIONS OF THE ROYAL SOCIETY A MATHEMATICAL, PHYSICAL & ENGINEERING SCIENCES

traverse, is of Oligocene age and runs in an E–W direction between the Tanggula and Kunlun mountains. The second was identified by Coulon *et al.* (1986) in the Maquiang area SW of Yangbajain who dated the rocks by the ^{40}Ar–^{39}Ar technique as 15–10 Ma. The extent of this province is unknown. The third, which lies at its closest some 200 km west of the traverse (and which we attempted, but failed, to reach) was identified by early explorers (e.g. Norin 1946) and later by Landsat imagery (e.g. Sengör & Kidd 1979) and first described in detail by Deng (1978). Limited data suggest that this province became active about 5 Ma ago and remains active, the last recorded eruption being in 1951.

The Oligocene province was represented on the traverse by a trachytic volcanic neck about 200 m in diameter, which is exposed at Zangmaxikong, in the Fenghuoshan (north of Erdaogou), where it penetrates Palaeocene or early Eocene red-beds of the Qiangtang Terrane (figure 18, QPg1), and has been dated at 32 Ma (Harris, Xu, Lewis, Hawkesworth & Zhang, this volume). The rock consists of about 80% sanidine, 9% carbonated clinopyroxene, 8% biotite and accessory magnetite, apatite and zircon. Its composition is marked by moderate concentrations of incompatible HFS elements and extremely high values of the LIL elements, including potassium which exceeds 5 mass% in the analysed samples. Chondrite-normalized REE patterns are very steep (figure 19*b*). The undersaturated composition indicates a mantle source, the very low heavy REE content indicate low-degrees of melting with residual garnet, and the high LIL element content coupled with high $\delta^{18}O$ values indicate significant crustal assimilation.

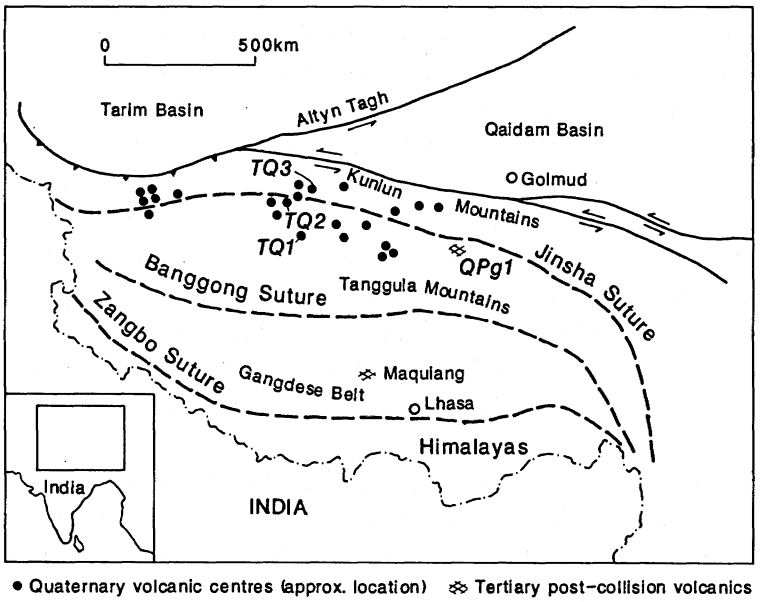

FIGURE 18. Distribution of recognized Tertiary post-collision volcanics on the Tibetan Plateau and locations of areas sampled.

The province, of which this trachyte is thought to be a part, extends from Zadoi county in Southern Qinghai through Muli and Yanbian counties in Western Sichuan to Yaoan county in Northern Yunnan. In all these areas, ages of around 30 Ma have been obtained and leucite lamproite-trachyte volcanic suites, often accompanied by syenite and alkali syenite intrusions, have been described.

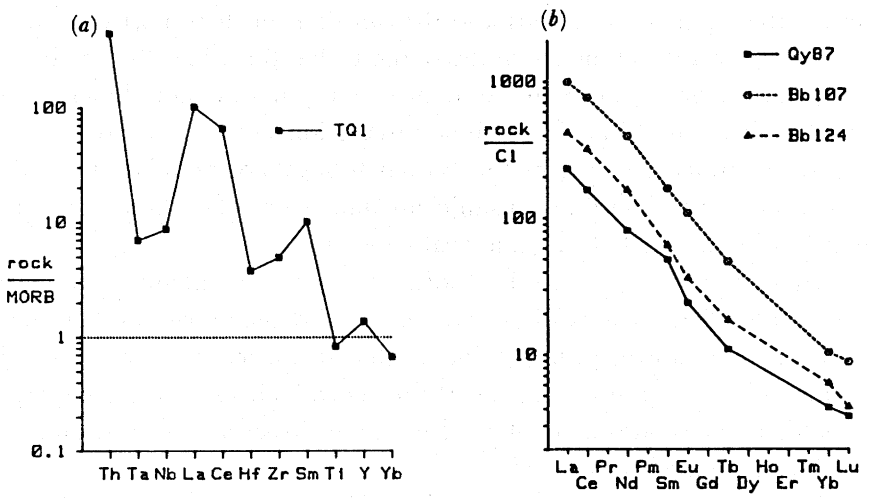

FIGURE 19. (*a*) MORB-normalized pattern and (*b*) chondrite-normalized REE plot for representative samples of Tertiary post-collision volcanics from the Tibetan plateau.

The Miocene volcanism at Maquiang described by Coulon *et al.* (1986) comprises a sequence of andesite–rhyolite flows and pyroclastic rocks. They are described as members of the high-K calc-alkaline series and have a composition which lies within the range of lavas from active continental margins: without an age it would be difficult to distinguish these rocks from their Linzizong precursors.

The NW Tibet Pliocene–Recent Province is, however, quite distinct geochemically. Trace element analyses of three of the samples described by Deng (1978) are given in table 1 and show extremely high concentrations of all incompatible elements, especially Sr, which exceeds 0.5% SrO_2 in some samples, and Zr. Samples from three areas were analysed by Deng (1978). The southernmost of these, in the Qiangtang Terrane, is the Bamaoqiongzong volcanic rock area (figure 18, TQ1) which contains potassic, ultra-alkaline rocks. The MORB-normalized pattern for one of the leucite foidites (figure 19*a*) is a typical post-collision type, closely resembling the ultrapotassic Alpine basalt (PCL4) in figure 2*d*. Its chondrite-normalized pattern shows extreme LREE enrichment, similar to that of the trachyte from Zangmaxikong. The central area (TQ2), also in the Qiangtang Terrane, is the Yongbocuo volcanic area, which contains both pyroxene dacites and trachyandesites. The northernmost area (TQ3), in the Kunlun Terrane, is the Qiangbaqian volcanic area, which contains mainly pyroxene andesites. The chondrite-normalized REE pattern for one of the andesites has been plotted in figure 19*b* and gives a steep pattern similar in shape to the two other samples plotted. These lavas do, however, contain significantly lower concentrations of the LIL elements (e.g. K, Rb, Sr, Th) than the lavas erupted further south (table 1).

The compositions of all the Oligocene–Recent volcanic rocks are characteristic of a highly enriched mantle source that contains major intraplate and subduction/assimilation components. The extremely high values of Sr indicate that the enrichment in LIL elements is due to subduction, rather than assimilation, since the latter would be expected to reduce, or have little effect on, Sr concentrations. This enrichment could have taken place by incorporation of a sialic melt into the sub-Tibetan lithosphere either during the Palaeogene collision event or during earlier subduction or collision events.

Although the precise implications of these observations for our understanding of the collision

event are not clear, the ages, compositions and distributions of these post-collision provinces may still place some constraints on the dynamics of the India–Eurasia collision. The Oligocene trachyte is far from any Palaeogene plate boundary so any mantle enrichment would either have to be inherited from the Triassic subduction-collision event or be the result of some 1000 km of northward underthrusting of the Indian lithosphere or relate to a hitherto unrecognized subduction event. There are insufficient data to resolve these three possibilities, although the first has by far the fewest geological constraints.

The Miocene Maquiang volcanics are less potassic (more calc-alkaline) in character and may simply have resulted from reactivation of the mantle wedge above the Palaeogene active continental margin. It may, however, be significant that this volcanic event occurs during the period of generation of leucogranites along the Main Central Thrust of the Himalayas (Debon *et al.* 1986): it could therefore also be explained by underthrusting of the Indian lithosphere northwards beneath the Gangdise belt.

The Pliocene–Recent volcanism in the NW of the Tibetan Plateau postdates by about 5 Ma the formation of leucogranites in the Kunlun (Molnar *et al.* 1987). The ultrapotassic composition of the volcanics could be explained by an inherited subduction component from the Triassic subduction–collision event, by subduction of the Indian lithosphere northwards, or by subduction of the Tarim basin lithosphere southwards. Of these possibilities, extensive Tibetan underplating by the Indian lithosphere, as proposed, for example by Powell (1986), is much the least likely. According to this model, we would expect extensive volcanic activity over much of the Tibetan Plateau for much of the past 40 Ma. The apparent absence of such activity suggests that any subduction of continental lithosphere was relatively recent. Moreover, the distribution of volcanic centres (figure 18) suggests that, if subduction did take place, it was directed from the north rather than the south. The geochemical polarity, particularly the increase in potassium towards the south, is also consistent with this model.

14. Summary and conclusions

The palaeotectonic information provided by the volcanic rocks of the Tibetan plateau can be summarized as follows.

1. *Devonian/Early Carboniferous active continental margin and/or post collision volcanism in the Northern Kunlun.* The interpretation of this extensive volcanic event is limited by poor age control and the superimposition of a major Triassic collision event. There is good geochemical evidence to suggest that these K-rich calc-alkaline volcanic rocks formed at an active continental margin or post-collision setting, or the transition from one to the other, but there is insufficient geological control to resolve these possibilities.

2. *Carboniferous arc volcanism in the southern Lhasa Terrane.* The sequence of basaltic to rhyolitic calc-alkaline volcanic rocks in the Dagze area east of Lhasa has the geological and geochemical characteristics of an arc volcano built up on transitional crust.

3. *Permian continental rift volcanism in the Qiangtang and Kunlun Terranes.* Permian rift volcanism is a characteristic of many terranes in China and SE Asia and is considered to represent a period of splitting of continental fragments from Eurasia by formation of new spreading centres. It is represented in the traverse area by extensive, mainly basaltic, volcanism south of Tuotuohe and around Naij Tal. The former exhibits geochemical characteristics of greater lithospheric attenuation (e.g. significant, and variable, crustal contamination and a less-enriched mantle

source) and may have been closer to a continental margin. Examples of still greater attenuation are, however, represented in the southern Kunlun Terrane east of the traverse area by a series of Permian submarine lavas, sill complexes and basic intrusions that, though not strictly ophiolitic, may represent incipient spreading.

4. *Triassic arc volcanism in the South Lhasa and Qiangtang Terranes*. Apparent active continental margin volcanism of Triassic age was identified north of Lhasa, although, as in the case of the Palaeozoic Kunlun volcanics, subsequent magmatic and tectonic events have masked any confirmatory geological evidence. Triassic volcanism is common throughout the Tethyan region where it may be either alkalic or, as in this area, calc-alkaline to shoshonitic (e.g. Pamič 1984): there is still much debate over whether the calc-alkaline volcanics owe their geochemical character to post-collision rifting of Hercynian terrain or whether they do represent a volcanic arc. The Batang Group north of Tuotuohe is, however, better constrained geologically and geochemically as an island arc developed on thin continental lithosphere. The presence of alkaline, as well as calc-alkaline, arc lavas further suggests the influence of a transform fault in the origin of the magmas, but the precise geometry cannot be determined without a more regional perspective. Southward subduction is consistent with the known distribution of sutures in the area.

5. *Permo–Triassic active continental margin volcanism in the Northern Kunlun*. Although no volcanic rocks of this age appear to be present, swarms of dykes cutting the Kunlun batholith probably fed now-eroded volcanoes. The composition of these calc-alkaline rocks could fit active continental margin or post-collision settings, but the evidence of a close temporal relationship with the pre-tectonic batholith makes the former much more probable.

6. *A Jurassic arc-basin complex in the North Lhasa Terrane*. The presence of volcanic rocks of clear island arc affinities south of Amdo and Dongqiao, coupled with the ophiolite evidence for marginal basin lithosphere discussed by Pearce & Deng (this volume), suggest that Jurassic northward intraoceanic subduction took place in the northern part of the Lhasa terrane, generating at a fore-arc/arc/back-arc complex which was emplaced as allochthonous slices during the formation of the Banggong Suture.

7. *A Jurassic back-arc or post-collision rift in the Qiangtang Terrane*. A minor basaltic volcanic event is recorded in Jurassic strata just north of Wenquan Station. Its setting and composition are equally consistent with an ensialic rifting event in a back-arc setting related to the Jurassic southward-directed subduction or in a post-collision setting related to the Triassic collision in the north.

8. *A Cretaceous post-collision volcanic event within and around the Banggong Suture*. The closure of the Banggong Suture was followed, after a time interval of 20 Ma or more, by a major outpouring of calc-alkaline to shoshonitic lavas and pyroclastic rocks across 200 km or more of the Geotraverse section for a period of some 30 Ma. Although the hypothesis of a subduction-related origin cannot be ruled out, the absence of any consistent time-space-composition relationships suggests to us that some, and perhaps all, of these lavas may be of post-collision origin. According to this model, the Takena Formation would have formed within a foreland basin related to the crustal thickening event that gave rise to this volcanic province.

9. *A Palaeogene active continental margin in the South Lhasa Terrane*. There is already a consensus that the calc-alkaline to shoshonitic Linzizong volcanics (and the Gangdise batholith) formed at an active continental margin related to the northward subduction of Tethyan lithosphere beneath Tibet. This work supports that consensus, but does note that the lavas at the top of

PHILOSOPHICAL TRANSACTIONS OF THE ROYAL SOCIETY A MATHEMATICAL, PHYSICAL & ENGINEERING SCIENCES

the sequence north of Lhasa and in the Yangbajain Rift may have more in common with volcanics in regions of intra-arc collision, than with arc volcanics *sensu stricto*.

10. *Oligocene–Recent post-collision volcanism on the Tibet Plateau.* The time-space distribution of post-collision volcanic activity on the Tibetan Plateau begins with the eruption of strongly undersaturated lavas in Central Tibet in Oligocene times, followed by 'typical' calc-alkaline volcanism in the southern part of the plateau in Miocene times and highly incompatible element enriched ultrapotassic volcanism in the NW of the plateau in Pliocene–Recent times. This sequence does not support wholesale underplating of the Tibetan plateau by continental lithosphere but is consistent with a limited amount of crust–mantle interaction by attempted subduction of continental lithosphere of India northwards and of the Tarim basin southwards as part of the crustal thickening event.

We are grateful to all the members of the Geotraverse team for their company and for geological discussions and to Dr P. J. Oakley and Mr P. Murray (Newcastle), Dr N. Rogers (Open University), R. Oliver (Grenoble), Li Sun-Rong and Bao Hui-Lan (Guiyang) and Zhao Yun-Long and Liang Yu-Tang (Beijing) for analytical work.

References

Bourgois, J. & Janjou, D. 1981 Subduction océanique, subduction continentale et surrection andine: l'example de Pérou septentrional. *C.R. Acad. Sci., Paris* **293**, 859–864.

Coulon, C., Maluski, H., Bollinger, C. & Wang, S. 1986 Mesozoic and Cenozoic volcanic rocks from central and southern Tibet: $^{40}Ar/^{39}Ar$ dating, petrological characteristics and geodynamical significance. *Earth planet. Sci. Lett.* **79**, 281–302.

Debon, F., Le Fort, P., Sheppard, S. M. F. & Sonet, J. 1986 The four plutonic belts of the Transhimalaya-Himalaya: a chemical, mineralogical, isotopic and chronological synthesis along a Tibet-Nepal section. *J. Petrol.* **27**, 219–250.

DeLong, S. E., Hodges, F. N. & Arculus, R. J. 1975 Ultramafic and mafic inclusions, Kanaga Island, Alaska and the occurrence of alkaline rocks in island arcs. *J. Geol.* **83**, 721–736.

Deng Wanming 1978 A preliminary study on the petrology and petrochemistry of the Quaternary volcanic rocks of northern Tibet autonomous region. *Acta. geol. Sinica* **52**, 148–162.

Ewart, A., Brothers, R. N. & Mateen, A. 1977 An outline of the geology and geochemistry, and the possible petrogenetic evolution of the volcanic rocks of the Tonga-Kermadec-New Zealand island arc. *J. Volcanol. geotherm. Res.* **2**, 205–250.

Frey, F. A. & Clague, D. A. 1983 Geochemistry of diverse basalt types from Loihi seamount: petrogenetic implications. *Earth planet. Sci. Lett.* **66**, 337–355.

Gorton, M. P. 1977 The geochemistry and origin of Quaternary volcanism in the New Hebrides. *Geochim. cosmochim. Acta* **41**, 1257–1270.

Holm, P. E. 1982 Non-recognition of continental tholeiites using the Ti–Zr–Y diagram. *Contr. Miner. Petr.* **79**, 308–310.

Hooper, P. R., Kleck, W. D., Knowles, C. R., Riedel, S. P. & Thiessen, R. L. 1984 Imaha basalt, Columbia River Basalt group. *J. Petrol.* **25**, 473–500.

Marriner, G. F. & Millward, D. 1984 The petrology and geochemistry of Cretaceous to Recent volcanism in Colombia: the magmatic history of an accretionary plate margin. *J. geol. Soc. Lond.* **141**, 473–486.

Mitchell, R. H. & Bell, K. 1976 Rare-earth geochemistry of potassic lavas from Birunga and Toro-Ankole regions of Uganda, Africa. *Contrib. Miner. Petr.* **58**, 293–303.

Molnar, P., Burchfiel, B. C., Zhao Ziyin, Liang K'uangyi, Wang Shuji & Huang Minmin 1987 Geological evolution of Northern Tibet: results of an expedition to Ulugh Muztagh. *Science, Wash.* **235**, 299–305.

Morrison, M. A., Thompson, R. N., Gibson, I. L. & Marriner, G. F. 1980 Lateral chemical heterogeneity in the Palaeocene upper mantle beneath the Scottish Hebrides. *Phil. Trans. R. Soc. Lond.* A **297**, 229–244.

Norin, E. 1946 Geological explorations in Western Tibet. In *Reports from the scientific expedition to the Northwestern provinces of China under the leadership of Dr. Sven Hedin.*, Publ. 29 (III), Geology 7. Tryckeri Aktiebolaget, Thule, Stockholm.

Pamič, J. J. 1984 Triassic magmatism of the Dinarides in Yugoslavia. *Tectonophysics* **109**, 273–307.

Pearce, J. A. 1984 The role of sub-continental lithosphere in magma genesis at active continental margins. In *Continental basalts and mantle xenoliths* (ed. C. J. Hawkesworth & M. J. Norry).

PHILOSOPHICAL TRANSACTIONS OF THE ROYAL SOCIETY A MATHEMATICAL, PHYSICAL & ENGINEERING SCIENCES

Pearce, J. A. & Cann, J. R. 1973 Tectonic setting of basic volcanic rocks determined using trace element analysis. *Earth planet. Sci. Lett.* **19**, 290–300.

Peccerillo, A. & Taylor, S. R. 1976 Geochemistry of Eocene calc-alkaline rocks from the Kastamonu area, northern Turkey. *Contr. Miner. Petr.* **58**, 63–81.

Powell, C. McA. 1986 Continental underplating model for the rise of the Tibetan Plateau. *Earth planet. Sci. Lett.* **81**, 79–94.

Riou, R., Dupuy, C. & Dostal, J. 1981 Geochemistry of coexisting alkaline and calk-alkaline volcanic rocks from Northern Azerbaijan (N.W. Iran). *J. Volcanol. geotherm. Res.* **11**, 253–275.

Rogers, N. W., Parker, R. J., Hawkesworth, C. J. & Marsh, J. S. 1985 The geochemistry of potassic lavas from Vulsini, central Italy and implications for mantle enrichment processes beneath the Roman region. *Contr. Miner. Petr.* **88**, 244–257.

Sengör, A. M. C. & Kidd, W. S. F. 1979 Post-collisional tectonics of the Turkish-Iranian Plateau and a comparison with Tibet. *Tectonophysics* **55**, 361–376.

Thompson, R. N., Morrison, M. A., Mattey, D. P., Dickin, A. P. & Moorbath, S. 1980 An assessment of the Th–Ta–Hf diagram as a discriminant for tectonomagmatic classifications and in the detection of crustal contamination of magmas. *Earth planet. Sci. Lett.* **50**, 1–10.

Thompson, R. N., Dickin, A. P., Gibson, I. L. & Morrison, M. A. 1982 Elemental fingerprints of isotopic contamination of Hebridean Palaeocene mantle-derived magmas by Archaean sial. *Contr. Miner. Petr.* **79**, 159–168.

Venturelli, G., Thorpe, R. S., Dal Piaz, G. V., Del Moro, A. & Potts, P. J. 1984 Petrogenesis of calc-alkaline, shoshonitic and associated ultrapotassic Oligocene volcanic rocks from the Northwestern Alps, Italy. *Contr. Miner. Petr.* **86**, 209–220.

Wang, S. 1980 Caracteristiques de la serie volcanique de Linzizong dans le secteur oriental de l'arc volcanique du Gangdese. In *Mission franco-chinois au Tibet 1980* (*C.N.R.S*), pp. 319–333.

Weaver, B. L. Wood, D. A., Tarney, J. & Joron, J. L. 1987 Geochemistry of ocean island basalts from the South Atlantic: Ascension, Bouvet, St. Helena, Gough and Tristan da Cunha. *Geol. Soc. Lond. spec. Paper.* no. 30, pp. 253–267.

Winchester, J. A. & Floyd, P. A. 1977 Geochemical discrimination of different magma series and their differentiation products using immobile elements. *Chem. Geol.* **20**, 325–343.

Wood, D. A., Joron, J.-L. & Treuil, M. 1979 A re-appraisal of the use of trace elements to classify and discriminate between magma series erupted in different tectonic settings. *Earth planet. Sci. Lett.* **45**, 326–336.

Yilmaz, Y., Saroglu, F. & Guner, Y. 1987 Initiation of the neomagmastism in East Anatolia. *Tectonophysics* **134**, 177–199.

Xu Ronghua, Sharer, U. & Allègre, C. J. 1985 Magmatism and metamorphism in the Lhasa Block (Tibet): an U-Pb geochronological study. *J. Geol.* **93**, 41–57.

Zhou Xinghua & Armstrong, R. L. 1982 Cenozoic volcanic rocks of eastern China-secular and geographic trends in chemistry and strontium isotopic composition. *Earth planet. Sci. Lett.* **58**, 301–329.

PHILOSOPHICAL TRANSACTIONS OF THE ROYAL SOCIETY A MATHEMATICAL, PHYSICAL & ENGINEERING SCIENCES

PHILOSOPHICAL TRANSACTIONS OF THE ROYAL SOCIETY A MATHEMATICAL, PHYSICAL & ENGINEERING SCIENCES

P

PEARCE & MEI

Appendix. Major and XRF / AA trace element data for Tibetan volcanics

Geochemical analyses for all analysed 'G' samples of volcanic rocks from the Geotraverse. Elements Zr, Y, Nb, Sr and Rb have been analysed by X-ray fluorescence and the remaining elements by atomic absorption. Key to rock sequences: L = Lhasa Terrane; Q = Qiangtang Terrane; K = Kunlun terrane; T = Tibet; Cb = Carboniferous; P = Permian; T = Triassic; J = Jurassic; C = Cretaceous; Pg = Palaeogene; Q = Quaternary. Key to rock types: bas. = basalt; and. = andesite; b/a. = basaltic andesite; sho. = shoshonite; p/b. = picrite basalt; rhy. = rhyolite; tra. = trachyte; bsn. = basanite; phn. = phonolite; L = lava; D = dyke; P = plug; S = sill; PL = pillow lava. Key to phenocrysts: ol = olivine; pl = plagioclase; cp = clinopyroxene; op = orthopyroxene; am = amphibole; bi = biotite; ks = K-feldspar; qz = quartz; aph = aphyric; alt = totally altered (gsch = greenschist; amph = amphibolite). See figures 5, 8, 11 and 14 in Pearce & Mei (this volume) for province locations and Kidd *et al.*, this volume (field slip, Microfiche 2, in pocket) for precise locations.

Appendix 1 : Major and XRF/AA trace element data for Tibetan volcanics.

Samp.	G14B	G16C	G16E	G16F	G32G	G32B	G36C	G36B	G36D
Prov.	LT1	LT1	LT1	LT1	LT2	LT2	LP1	LP1	LP1
No.	1	2	3	4	1	2	1	2	3
RType	Pc	L	L	L	L	Sp	L	L	L
SiO2	50.20	50.00	52.00	57.80	48.70	51.20	53.20	56.70	60.20
TiO2	.91	1.12	1.03	.92	.92	.91	.83	.80	.80
Al2O3	16.70	17.10	17.00	13.20	14.60	18.50	21.00	18.00	16.50
Fe2O3	8.99	10.50	9.06	8.38	7.94	8.76	6.52	7.58	5.86
MnO	.14	.18	.17	.19	.17	.18	.07	.18	.15
MgO	7.22	4.79	5.74	7.72	4.39	5.12	3.33	3.95	4.26
CaO	8.04	7.49	9.61	10.10	10.80	6.08	7.34	7.66	7.06
Na2O	4.15	4.29	3.95	1.66	2.14	5.30	4.99	2.69	2.56
K2O	.40	.60	.10	.16	1.05	.48	.42	1.26	.64
P2O5	.16	.42	.23	.39	.25	.20	.16	.17	.13
LOI	2.74	3.87	1.41	.55	9.31	3.71	2.69	1.73	2.23
Total	99.65	100.36	100.30	101.07	100.27	100.44	100.55	100.72	100.39
Zr	55	145	88	92	125	88	146	125	146
Y	16	24	22	24	23	25	17	21	18
Nb	4.0	0.0	5.8	8.0	3.9	0.0	5.0	6.4	7.1
Rb	13	12	2.8	0.0	49	22	8.5	19	18
Sr	220	731	502	809	914	716	603	430	833
Cr	260	83	150	440	83	22	35	38	38
Ni	85	34	39	115	16	13	21	22	25
V	280	440	290	250	210	270	190	220	163
Cu	75	47	21	140	15	53	30	21	59
Zn	79	82	83	68	82	101	100	85	85
Th	0.0	0.0	0.0	0.0	17	21	5.6	4.1	8.1
Sc	30	28	29	29	28	28	18	23	19
Pheno-crysts		ol	pl,cp	pl,cp	pl,cp	pl,cp	pl,am	aph	aph

PHILOSOPHICAL TRANSACTIONS OF THE ROYAL SOCIETY A MATHEMATICAL, PHYSICAL & ENGINEERING SCIENCES

Appendix 1 : Major and XRF/AA trace element data for Tibetan volcanics.

Samp.	G36A	G46C	G46B	G107D	G106A	G107A	G106D	G130E	G130C
Prov.	LP1	LP2	LP2	LJ1	LJ1	LJ1	LJ1	LJ2	LJ2
No.	4	1	2	1	2	3	4	1	2
RType	L	L	L	PL	PL	PL	PL	L	L
SiO2	67.40	53.50	64.40	38.40	42.80	47.40	47.60	49.50	50.60
TiO2	.37	.84	.77	.55	.58	.67	.56	.52	.56
Al2O3	15.10	19.70	16.70	10.60	11.60	13.40	11.20	14.30	15.30
Fe2O3	1.70	6.22	4.34	6.56	7.53	8.30	6.20	8.83	9.37
MnO	.04	.13	.06	.25	.37	.25	.15	.15	.17
MgO	.70	1.75	.42	4.21	4.00	6.84	5.04	7.44	8.97
CaO	5.00	4.27	1.37	20.30	16.10	10.40	15.90	12.60	9.59
Na2O	4.78	4.12	3.65	3.95	3.82	4.46	3.51	1.23	2.11
K2O	1.06	6.00	7.37	.34	.48	.18	.68	.18	.43
P2O5	.10	.42	.17	.10	.12	.09	.09	.07	.08
LOI	4.49	3.60	.71	14.10	12.70	8.13	9.98	3.77	3.42
Total	100.74	100.55	99.96	99.36	100.10	100.12	100.91	98.59	100.60
Zr	105	401	642	31	33	38	32	33	26
Y	7	35	47	15	13	14	11	13	13
Nb	2.3	24	40	0.0	3.0	0.0	2.4	2.2	2.0
Rb	57	142	371	4.7	13	3.1	13	0.0	6.0
Sr	456	99	281	169	173	123	157	324	442
Cr	10	2	2	660	680	600	480	220	340
Ni	12	8	6	168	173	206	217	58	88
V	58	88	41	150	150	210	180	0	290
Cu	148	42	9	22	23	34	35	118	152
Zn	37	93	74	54	60	70	51	68	74
Th	0.0	39	69	0.0	0.0	0.0	0.0	0.0	0.0
Sc	6	5	5	25	25	29	28	0	43
Pheno-crysts	aph	ks	pl,bi ks	pl,cp	pl,cp	pl,cp	pl,cp	pl,cp	pl,cp

PHILOSOPHICAL TRANSACTIONS OF THE ROYAL SOCIETY A MATHEMATICAL, PHYSICAL & ENGINEERING SCIENCES

Appendix 1 : Major and XRF/AA trace element data for Tibetan volcanics.

Samp.	G130A	G130B	G129A	G126F	G128C	G55F	G55E	G55G	G55B
Prov.	LJ2	LJ2	LJ2	LJ2	LJ2	LC1	LC1	LC1	LC1
No.	3	4	5	6	7	1	2	3	4
RType	L	L	L	L	L	L	L	L	L
SiO2	65.70	71.00	74.20	74.60	73.40	51.80	52.10	53.50	62.20
TiO2	.67	.76	.54	.06	.32	.81	.88	.87	1.01
Al2O3	14.30	12.30	12.90	14.40	12.70	14.80	15.00	15.20	16.60
Fe2O3	5.34	5.15	2.99	.92	2.38	8.13	7.22	8.35	5.32
MnO	.08	.06	.03	.01	.04	.12	.15	.13	.07
MgO	2.75	2.35	.64	.38	.64	6.03	5.54	7.85	.54
CaO	4.38	2.95	1.38	.22	1.90	10.20	11.70	8.92	3.37
Na2O	4.54	3.92	4.99	.16	3.96	2.06	2.20	2.35	3.73
K2O	.18	.88	1.32	7.52	3.54	1.54	1.38	1.67	5.10
P2O5	.12	.26	.06	.01	.02	.17	.20	.19	.33
LOI	2.27	1.04	1.12	1.60	1.35	4.71	3.78	1.68	2.27
Total	100.33	100.67	100.17	99.88	100.25	100.37	100.15	100.71	100.54
Zr	162	101	230	78	144	100	114	109	311
Y	33	41	50	19	41	19	21	20	31
Nb	3.5	2.0	4.0	10	13	6.5	7.4	6.6	7.4
Rb	0.0	14	0.0	412	40	59	44	71	240
Sr	162	286	147	29	154	289	324	309	389
Cr	43	2	5	0	10	480	540	460	7
Ni	18	4	2	10	9	91	141	83	3
V	136	44	30	11	29	190	220	220	110
Cu	27	6	14	0	0	29	45	17	6
Zn	58	85	44	26	31	72	84	76	62
Th	3.5	0.0	3.9	19	21	12	13	13	35
Sc	14	16	9	5	9	25	24	25	10
Pheno-crysts	ol,pl cp	pl	pl			ol,pl cp	ol,pl cp,op	ol,pl cp	ol,pl cp

PHILOSOPHICAL TRANSACTIONS OF THE ROYAL SOCIETY A MATHEMATICAL, PHYSICAL & ENGINEERING SCIENCES

Appendix 1 : Major and XRF/AA trace element data for Tibetan volcanics.

Samp.	G55A	G99B	G84	G88	G85B	G86B	G98C	G87A	G133H
Prov.	LC1	LC3	LC3	LC3	LC3	LC3	LC3	LC3	LC4
No.	5	1	2	3	4	5	6	7	1
RType	L	L	D	L	L	L	L	L	L
SiO2	62.80	53.60	53.70	55.40	55.60	58.60	65.00	72.80	54.40
TiO2	1.11	.94	1.20	.87	.90	.77	.67	.24	2.12
Al2O3	16.90	15.80	16.10	17.00	18.10	15.10	16.10	13.60	15.80
Fe2O3	4.54	8.09	7.14	8.09	7.46	6.45	5.05	1.83	8.98
MnO	.04	.13	.10	.12	.10	.11	.10	.01	.08
MgO	.68	3.93	4.74	3.70	3.59	6.39	2.63	.22	4.76
CaO	2.74	7.01	4.92	6.09	6.52	2.48	5.33	1.21	5.46
Na2O	3.50	2.79	3.98	4.36	2.99	5.32	3.23	.96	3.41
K2O	5.14	2.13	2.28	2.36	1.60	.14	1.04	9.47	.30
P2O5	.33	.17	.26	.15	.19	.12	.14	.03	.35
LOI	1.95	5.65	5.49	2.09	2.68	4.62	1.19	.57	4.13
Total	99.73	100.24	99.91	100.23	99.73	100.10	100.48	100.94	99.79
Zr	334	158	225	147	209	154	198	268	318
Y	32	26	23	25	30	21	28	36	36
Nb	19	10	13	8.5	11	7.9	13	23	10
Rb	209	91	79	116	111	8.0	65	500	7.3
Sr	407	434	403	391	451	126	488	24	300
Cr	8	57	220	64	29	130	25	2	51
Ni	3	16	47	16	10	22	7	4	15
V	110	6	140	190	200	160	100	20	210
Cu	6	32	22	10	9	7	13	6	24
Zn	105	94	69	82	98	118	66	8	129
Th	33	6.0	15	14	18	15	27	42	9.1
Sc	9	19	18	21	19	19	14	5	24
Pheno-crysts	ol,pl	pl	aph	pl,cp ol	pl,cp ol,mt	pl,cp mt	ol,pl	pl	ol,pl

PHILOSOPHICAL TRANSACTIONS OF THE ROYAL SOCIETY A MATHEMATICAL, PHYSICAL & ENGINEERING SCIENCES

Appendix 1 : Major and XRF/AA trace element data for Tibetan volcanics.

Samp.	G133B	G133D	G133G	G133J	G138E	G138D	G138C	G138H	G138I
Prov.	LC4	LC4	LC4	LC4	QJ1	QJ1	QJ1	QJ1	QJ1
No.	2	3	4	5	1	2	3	4	5
RType	L	L	L	L	L	L	L	L	D
SiO2	57.80	51.60	55.90	54.50	45.70	47.70	51.20	53.10	43.90
TiO2	1.95	1.84	1.75	2.12	1.44	1.32	1.40	1.64	1.07
Al2O3	13.50	18.00	14.90	15.70	16.80	16.20	17.80	16.80	16.00
Fe2O3	8.56	7.92	9.30	8.76	11.00	8.91	10.50	11.10	9.59
MnO	.10	.09	.09	.18	.14	.13	.07	.06	.12
MgO	2.14	3.20	2.42	3.39	8.31	1.36	1.81	5.36	4.31
CaO	3.93	6.58	4.92	8.25	7.07	8.79	4.24	2.00	6.84
Na2O	5.67	4.24	4.86	3.71	3.44	6.51	6.25	5.83	3.65
K2O	.78	2.00	.36	1.03	1.12	.84	1.05	.48	.66
P2O5	.51	.46	.39	.35	.22	.47	.56	.49	.23
LOI	4.38	4.57	5.69	3.04	4.78	7.91	6.23	3.93	12.62
Total	99.32	100.50	100.58	101.03	100.02	100.14	101.11	100.79	98.99
Zr	387	337	274	307	117	171	187	187	168
Y	43	44	32	36	26	18	26	25	34
Nb	21	18	15	11	4.1	11	12	11	6.3
Rb	6.9	13	11	29	59	57	58	21	13
Sr	279	500	146	334	189	364	172	131	328
Cr	19	28	30	45	340	160	160	200	350
Ni	14	16	19	12	97	57	30	59	54
V	131	184	191	210	250	190	190	280	209
Cu	27	151	33	17	7	12	11	8	2
Zn	60	80	50	140	152	54	56	83	82
Th	17	14	14	5.8	0.0	4.3	6.3	3.1	4.8
Sc	15	14	13	24	31	18	14	13	24
Pheno-crysts	ol,pl	ol,pl	ol,pl	ol,pl	ol	aph	aph	aph	aph

PHILOSOPHICAL TRANSACTIONS OF THE ROYAL SOCIETY A MATHEMATICAL, PHYSICAL & ENGINEERING SCIENCES

Appendix 1 : Major and XRF/AA trace element data for Tibetan volcanics.

Samp.	G151E	G151D	G150E	G152J	G152C	G152A	G152D	G150B	G150C
Prov.	QP1	QP1	QP1	QP1	QP1	QP1	QP1	QP2	QP2
No.	1	2	3	4	5	6	7	1	2
RType	L	L	L	L	L	Br	L	L	L
SiO2	48.40	50.10	53.80	54.20	55.30	57.60	58.20	49.00	50.10
TiO2	1.86	1.60	.80	1.31	1.22	.90	1.00	2.19	2.01
Al2O3	16.10	17.30	17.60	18.40	19.00	16.90	17.30	14.80	14.70
Fe2O3	10.80	9.53	6.73	7.52	9.28	6.75	5.60	13.20	11.90
MnO	.19	.16	.13	.11	.10	.13	.10	.70	.34
MgO	8.71	5.42	2.63	2.24	3.06	3.67	2.65	6.40	6.36
CaO	6.94	7.78	5.82	4.35	1.81	4.75	5.38	6.84	7.63
Na2O	3.93	4.83	7.29	7.70	7.12	4.55	5.86	2.02	3.72
K2O	.18	.38	.32	.22	.56	.76	1.85	1.44	.72
P2O5	.28	.43	.22	.76	.54	.35	.41	.25	.21
LOI	3.58	3.22	4.67	4.02	1.98	4.16	2.61	2.74	2.37
Total	100.97	100.75	100.01	100.83	99.97	100.52	100.96	99.58	100.06
Zr	144	149	35	226	187	174	148	129	122
Y	29	25	15	22	12	12	15	33	28
Nb	7.9	15	2.7	20	17	12	14	5.4	7.0
Rb	3.5	8.6	9.5	46	15	19	40	9.5	20
Sr	913	613	396	462	968	651	1075	302	294
Cr	200	124	2	47	50	32	36	180	178
Ni	110	94	2	42	31	28	30	68	59
V	270	230	0	170	170	160	160	355	338
Cu	53	9	61	13	12	9	7	43	44
Zn	121	90	205	120	212	690	149	490	195
Th	2.7	2.6	0.0	4.7	7.6	4.2	6.8	0.0	14
Sc	18	23	0	16	6	13	14	23	16
Pheno-crysts	aph	aph	aph	aph	aph	pl	aph	,aph	aph

PHILOSOPHICAL TRANSACTIONS OF THE ROYAL SOCIETY A MATHEMATICAL, PHYSICAL & ENGINEERING SCIENCES

Appendix 1 : Major and XRF/AA trace element data for Tibetan volcanics.

Samp.	G154I	G154F	G154L	G154D	G154A	G154K	G154N	G153E	G153A
Prov.	QT1	QT1	QT1	QT1	QT1	QT1	QT1	QT2	QT2
No.	1	2	3	4	5	6	7	1	2
RType	L	L	L	L	L	L	L	L	L
SiO2	49.30	51.30	51.50	53.30	53.80	44.60	50.40	53.40	58.60
TiO2	1.04	1.00	.78	.97	.96	.99	1.16	.84	.64
Al2O3	18.7	18.80	21.40	17.80	18.00	17.40	18.40	21.30	19.00
Fe2O3	9.06	9.07	7.99	8.72	8.15	10.40	10.50	7.54	6.12
MnO	.23	.23	.12	.15	.15	.26	.12	.09	.07
MgO	2.83	3.58	2.60	3.52	2.62	4.09	2.48	1.60	1.00
CaO	8.34	8.72	9.94	5.50	7.93	11.10	7.62	6.32	2.67
Na2O	2.99	3.14	3.62	3.96	3.19	2.24	4.74	5.80	8.01
K2O	2.53	2.63	.46	3.80	2.92	2.36	1.06	1.04	.64
P2O5	.46	.45	.09	.34	.41	.32	.33	.18	.17
LOI	4.75	2.20	1.81	2.46	1.90	7.15	3.27	2.67	2.35
Total	100.23	101.12	100.31	100.52	100.03	100.91	100.08	100.78	99.27
Zr	131	207	108	202	133	87	206	94	8
Y	21	25	26	26	24	23	74	20	4
Nb	23	25	4.1	27	21	19	4.8	4.0	1.8
Rb	56	101	6.1	102	71	19	2.6	26	59
Sr	462	526	141	491	594	433	87	344	296
Cr	3	6	7	21	7	29	15	2	2
Ni	6	12	7	9	6	18	16	4	5
V	280	240	280	210	210	330	248	150	93
Cu	22	38	17	15	38	26	17	10	5
Zn	198	103	87	86	79	153	85	120	85
Th	12	18	0.0	20	13	9.4	0.0	4.0	0.0
Sc	25	20	28	20	18	24	31	22	8
Pheno-crysts	ol,pl	ol,pl cp	ol,pl cp	ol,pl cp	ol,pl cp			ol,pl	

PHILOSOPHICAL TRANSACTIONS OF THE ROYAL SOCIETY A MATHEMATICAL, PHYSICAL & ENGINEERING SCIENCES

Appendix 1 : Major and XRF/AA trace element data for Tibetan volcanics.

Samp.	G153C	G153G	G216E	G216I	G216C	G228F	G228A	G216A	G217A
Prov.	QT2	QT2	KP1	KP1	KP1	KP1	KP1	KP1	KP1
No.	3	4	1	2	3	4	5	6	7
RType	L	L	L	L	L	L	L	L	L
SiO2	43.80	55.60	41.00	47.20	48.20	48.40	48.80	49.00	49.80
TiO2	.73	.83	4.60	3.54	3.33	3.72	3.88	3.57	1.89
Al2O3	12.90	17.80	15.00	14.40	12.90	15.20	15.40	12.80	14.00
Fe2O3	7.60	6.48	18.50	14.90	15.70	11.70	12.50	16.20	13.60
MnO	.31	.07	.24	.19	.23	.16	.18	.23	.22
MgO	4.45	.80	6.17	5.46	5.54	2.96	4.26	5.32	6.24
CaO	13.43	5.46	10.50	10.10	10.10	8.26	9.02	10.30	10.30
Na2O	3.49	6.74	1.38	2.58	2.91	5.60	4.01	2.35	3.01
K2O	.06	.64	.16	.73	.62	1.07	.90	.38	.14
P2O5	.14	.08	.47	.34	.32	.54	.39	.39	.13
LOI	12.37	5.13	1.80	.78	.25	3.03	.89	.44	1.13
Total	99.28	99.63	99.82	100.22	100.10	100.64	100.23	100.98	100.46
Zr	71	33	347	257	235	364	329	268	98
Y	20	19	46	36	34	38	37	38	21
Nb	3.5	3.2	28	23	24	50	47	26	6.5
Rb	1.4	3.7	2.3	18	20	13	29	7.9	1.1
Sr	146	100	413	152	291	345	469	546	409
Cr	10	3	260	240	61	13	87	66	53
Ni	9	5	109	125	49	31	51	43	72
V	120	126	520	430	460	330	290	460	370
Cu	398	22	268	198	211	11	0	253	84
Zn	77	112	171	133	147	97	113	151	129
Th	0.0	0.0	3.8	0.0	5.2	5.1	2.0	3.8	0.0
Sc	14	21	45	36	23	25	25	25	33
Pheno-crysts			aph		alt gsch	aph	pl	aph	alt amph

PHILOSOPHICAL TRANSACTIONS OF THE ROYAL SOCIETY A MATHEMATICAL, PHYSICAL & ENGINEERING SCIENCES

Appendix 1 : Major and XRF/AA trace element data for Tibetan volcanics.

Samp.	G229A	G217D	G254C	G253E	G253M	G253L	G253I	G254F	G253S
Prov.	KP1	KP1	KD1	KD1	KD1	KD1	KD1	KD1	KD1
No.	8	9	1	2	3	4	5	6	7
RType	L	L	L	L	L	L	L	L	L
SiO2	50.00	63.50	45.90	47.80	50.20	50.40	51.60	54.00	56.00
TiO2	3.10	.46	1.10	1.22	2.03	.98	1.50	.77	.97
Al2O3	14.00	16.50	22.40	18.40	16.10	15.30	17.70	15.50	16.90
Fe2O3	14.00	4.83	10.40	10.30	10.30	9.50	9.74	6.74	9.33
MnO	.21	.08	.23	.20	.16	.19	.15	.14	.17
MgO	4.52	2.59	4.20	6.66	6.59	10.10	7.66	3.24	4.29
CaO	10.20	7.11	8.93	10.80	9.29	10.60	5.16	7.40	8.10
Na2O	3.24	3.07	2.93	2.12	3.50	1.48	4.16	2.58	2.50
K2O	.72	1.20	.60	1.54	1.25	1.28	2.10	2.33	1.35
P2O5	.29	.48	.21	.20	.29	.12	.25	.12	.13
LOI	.70	.22	2.71	.80	1.23	1.06	.72	7.78	.64
Total	100.98	100.04	99.61	100.04	100.94	101.01	100.74	100.60	100.38
Zr	228	336	170	95	214	79	222	206	140
Y	37	19	34	21	37	19	30	36	26
Nb	18	23	7.7	6.9	8.6	6.6	6.5	11	6.5
Rb	21	41	24	123	54	68	152	100	65
Sr	329	444	336	339	349	208	288	193	212
Cr	115	2	15	32	200	640	104	43	9
Ni	64	7	80	12	38	125	29	3	8
V	410	81	20	270	170	260	170	87	220
Cu	181	33	33	17	15	40	5	14	35
Zn	137	74	123	157	110	89	148	95	102
Th	2.2	6.7	5.0	5.3	5.4	0.0	0.0	12	9.3
Sc	33	10	24	30	24	33	23	20	24
Pheno-crysts	alt amph	alt gsch	pl,am	pl			pl,am	pl,am	pl,cp bi

PHILOSOPHICAL TRANSACTIONS OF THE ROYAL SOCIETY A MATHEMATICAL, PHYSICAL & ENGINEERING SCIENCES

Appendix 1 : Major and XRF/AA trace element data for Tibetan volcanics.

Samp.	G253W	G253H	G250C	G250F	G250D	G250G	G250A	G255B	G250B
Prov.	KD1	KD1	KD2	KD2	KD2	KD2	KD2	KD2	KD2
No.	8	9	1	2	3	4	5	6	7
RType	L	L	L	L	L	L	Pc	Pc	Pc
SiO2	65.90	69.10	53.60	58.30	59.20	60.00	66.40	68.80	70.60
TiO2	.93	.49	1.03	.77	1.07	.81	.49	.34	.38
Al2O3	15.10	15.90	18.60	17.80	17.90	16.70	15.80	15.70	14.80
Fe2O3	6.23	3.18	9.34	8.83	7.66	7.24	5.59	3.51	3.16
MnO	.08	.05	.17	.15	.13	.12	.10	.08	.09
MgO	1.94	2.14	3.64	3.01	2.35	3.04	2.08	.38	.74
CaO	3.79	2.10	7.68	6.01	6.97	6.46	2.16	2.51	2.60
Na2O	3.69	6.40	2.60	2.78	2.41	2.98	2.80	4.53	3.68
K2O	2.77	.96	1.14	.87	1.49	1.80	2.70	2.93	2.70
P2O5	.24	.10	.19	.13	.27	.13	.10	.08	.08
LOI	.52	.51	2.62	1.12	1.33	1.00	2.05	1.19	1.94
Total	100.79	100.93	100.61	99.77	100.78	100.28	100.27	100.05	100.77
Zr	376	178	198	155	147	174	276	386	168
Y	36	13	31	31	24	25	32	30	18
Nb	11	3.7	9.7	7.0	8.9	8.8	14	11	9.6
Rb	149	36	60	35	69	76	124	138	112
Sr	153	362	259	227	304	248	284	246	284
Cr	9	51	30	32	7	77	9	8	9
Ni	2	14	9	14	6	18	5	2	6
V	41	67	150	180	130	190	57	17	59
Cu	5	11	17	9	26	45	6	9	5
Zn	99	70	106	84	81	75	120	110	65
Th	12	0.0	8.3	11	7.2	14	17	20	16
Sc	14	6	21	20	15	21	9	6	6
Pheno-crysts	aph	pl	pl,am			pl,am	pl,ks qz		am,ks qz

PHILOSOPHICAL TRANSACTIONS OF THE ROYAL SOCIETY A MATHEMATICAL, PHYSICAL & ENGINEERING SCIENCES

Appendix 1 : Major and XRF/AA trace element data for Tibetan volcanics.

Samp.	G250E	G258A	G259C	G258C	G252	G248E	G239B	G255C	G259B
Prov.	KD2	KD2	KT1	KT1	KT1	KT1	KT1	KT1	KT1
No.	8	9	1	2	3	4	5	6	7
RType	Pc	Pc	D	D	D	D	D	D	D
SiO2	71.70	78.00	47.30	56.40	59.70	60.50	62.60	54.70	61.60
TiO2	.38	.12	1.23	.93	.87	1.34	.63	.90	.73
Al2O3	15.10	12.00	17.50	19.60	16.10	16.20	16.80	17.40	17.00
Fe2O3	3.13	1.90	9.33	7.38	8.36	7.65	6.67	9.26	6.30
MnO	.07	.01	.19	.12	.18	.16	.14	.16	.12
MgO	.66	.26	5.59	1.93	1.35	2.36	1.53	3.49	2.87
CaO	2.65	.38	9.07	6.25	4.99	5.64	4.76	8.56	5.46
Na2O	3.82	1.36	1.92	4.42	2.74	3.67	4.02	2.79	3.31
K2O	2.81	6.04	1.26	1.15	3.16	1.73	1.63	1.22	1.75
P2O5	.08	.02	.23	.18	.25	.34	.29	.13	.18
LOI	.78	.92	6.10	1.99	2.63	.43	1.67	1.48	1.02
Total	101.18	101.01	99.72	100.35	100.33	100.02	100.74	100.09	100.34
Zr	174	145	119	155	250	225	190	135	179
Y	18	27	19	26	40	21	23	25	20
Nb	10	9.6	5.9	7.3	12	11	10	7.8	9.8
Rb	119	233	86	33	178	70	97	50	56
Sr	242	92	415	402	276	319	429	346	445
Cr	10	6	59	13	7	8	6	16	22
Ni	2	3	7	6	2	2	2	7	7
V	39	12	230	150	54	97	36	199	113
Cu	6	6	27	41	12	12	6	96	14
Zn	48	35	135	86	400	87	60	102	84
Th	18	28	4.3	7.6	15	7.3	6.7	6.5	6.7
Sc	6	5	25	15	16	18	3	25	18
Pheno-crysts	am,bi ks,qz		aph		aph				

PHILOSOPHICAL TRANSACTIONS OF THE ROYAL SOCIETY A MATHEMATICAL, PHYSICAL & ENGINEERING SCIENCES

Appendix 1 : Major and XRF/AA trace element data for Tibetan volcanics.

Samp.	G253Y
Prov.	KT1
No.	8
RType	D
SiO2	54.20
TiO2	2.45
Al2O3	15.20
Fe2O3	12.50
MnO	.17
MgO	3.62
CaO	2.45
Na2O	2.47
K2O	6.08
P2O5	.67
LOI	.49
Total	100.30
Zr	1793
Y	58
Nb	16
Rb	231
Sr	180
Cr	23
Ni	4
V	150
Cu	10
Zn	161
Th	14
Sc	14
Pheno-crysts	pl

PHILOSOPHICAL TRANSACTIONS OF THE ROYAL SOCIETY A MATHEMATICAL, PHYSICAL & ENGINEERING SCIENCES